

DIMENSION REDUCTION FOR STOCHASTIC OSCILLATORS:
INVESTIGATING COMPETING GENERALIZATIONS OF
PHASE AND ISOCHRONS

by

ALEXANDER CAO

Submitted in partial fulfillment of the requirements

for the degree of Master of Science

Thesis Advisor: Prof. Peter Thomas

Department of Mathematics, Applied Mathematics, and Statistics

CASE WESTERN RESERVE UNIVERSITY

May 2017

CASE WESTERN RESERVE UNIVERSITY

SCHOOL OF GRADUATE STUDIES

We hereby approve the thesis of

Alexander Cao

candidate for the degree of Master of Science *.

Prof. Peter Thomas (Committee chair)

Prof. Joel Langer

Prof. Wojbor Woyczynski

Prof. Benjamin Lindner (External faculty)

(date) March 8, 2017

*We also certify that written approval has been obtained for any
proprietary material contained therein.

Contents

List of Figures	v
Acknowledgements	viii
List of Abbreviations	ix
Abstract	x
1 Introduction	1
1.1 Average Isophase [1]	3
2 Mean First-Passage Time Problem	5
2.1 One-Dimensional and Planar Diffusion	6
3 Extending Average Isophase [1] in One-Dimension	8
3.1 Trivial System	10
3.2 Tilted Periodic Potential	15
3.3 Solvability Condition for the PDE Problem	16

4	Extending Average Isophase [1] in Planar Systems	22
4.1	Noisy, Heteroclinic Oscillator [2]	22
4.2	Generalized Stuart-Landau Oscillator [3]	29
4.3	Noisy Stuart-Landau Oscillator with y -polarized Noise [1]	34
4.4	Solvability Condition for the PDE Problem	38
5	(Non)Equivalence of Average Isophase [1] and Spectral Phase [2]	43
5.1	Spectral Phase [2]	43
5.2	(Non)Equivalence in One-Dimension	45
5.3	(Non)Equivalence in Planar Systems	48
6	Discussion	49
6.1	Extending Average Isophase [1]	49
6.2	Limitations of the PDE Approach	50
6.3	Relation Between Stationary Flux and Mean Period	51
6.4	(Non)Equivalence of Average Isophase [1] and Spectral Phase [2]	55

7 Conclusion	56
A Appendix	58
A.1 Matlab Code for MFPT Calculation of Heteroclinic System [2]	58
References	63

List of Figures

1	One-dimensional diffusion realizations and MFPT	7
2	Planar diffusion realizations and MFPT	9
3	Trivial system realizations and <i>true</i> MFPT	11
4	Trivial system MFPT with periodic boundaries	11
5	Trivial system MFPT with left reflecting boundary	12
6	Trivial system MFPT with <i>extended</i> left reflecting boundary .	14
7	Trivial system MFPT with “jump” boundary condition	15
8	Tilted periodic potential realization	16
9	Tilted periodic potential MFPT with “jump” and extended left boundary conditions	17
10	Noisy, heteroclinic oscillator realization	23
11	Noisy, heteroclinic oscillator on multiple copies of domain . . .	24
12	Noisy, heteroclinic oscillator “time crystal” structure	26
13	Noisy, heteroclinic oscillator finite difference scheme	27

14	Noisy, heteroclinic oscillator MFPT and average isophases . . .	28
15	Generalized Stuart-Landau finite difference scheme	30
16	Isochronal clock model realization	31
17	Isochronal clock model MFPT and average isophases	31
18	Counterrotating realization	32
19	Antirrotating realization	32
20	Counterrotating case MFPT and average isophases	33
21	Antirrotating case MFPT and average isophases	34
22	Noisy Stuart-Landau oscillator with y -polarized noise trajectory	35
23	Noisy Stuart-Landau oscillator with y -polarized noise finite dif- ference scheme and deterministic phase portrait	36
24	Noisy Stuart-Landau oscillator with y -polarized noise MFPT and average isophases	37
25	Noisy Stuart-Landau oscillator with y -polarized noise isophase and “spoke”	38
26	MFRTs of isophase and “spoke” calculated from MC simula- tions for noisy Stuart-Landau oscillator with y -polarized noise	39

27	Heteroclinic system stationary distribution	56
----	---	----

Acknowledgements

I would like to thank Professor Thomas for all his mentorship and guidance through the years. I would also like to thank Professor Lindner for his contributions and useful discussions. Finally, I would like to thank Professors Langer and Woyczynski for serving on my MS thesis committee.

This work was supported by a grant from the Arthur I. Mendolia '41 Fellowship from the Case Alumni Foundation and by National Science Foundation grant DMS-1413770.

This work made use of the High Performance Computing Resource in the Core Facility for Advanced Research Computing at Case Western Reserve University.

List of Abbreviations

SDE stochastic differential equation

PDE partial differential equation

MFPT mean first-passage time

MFRT mean first-return time

MC Monte Carlo

Abstract

Dimension reduction for stochastic oscillators:

Investigating competing generalizations of phase and isochrons

Abstract

by

Alexander Cao

A stable, finite-period limit cycle in a deterministic system has a set of Poincaré sections with two properties: all trajectories with initial conditions on a given leaf (i) converge to a common trajectory on the limit cycle and (ii) pass through the same leaf after an interval equalling one period. The leaves are the isochrons, and the timing of their movement defines the asymptotic phase of points converging to the limit cycle. In a Markovian stochastic setting, two generalizations of the asymptotic phase and the isochron foliation have been proposed. One is based on the spectral decomposition of the Kolmogorov Backward operator and the other on foliations defined by a uniform mean first-passage time property. We extend the latter generalization by reformulating the established numerical procedure for calculating the leaves in terms of a partial differential equation. We also discuss the (non)equivalence of these two phase generalizations for noisy oscillators.

1 Introduction

Oscillations, or rhythmic phenomena, are found throughout the natural world. Examples include swallowing [4], breathing [5, 6], neuronal motor control circuits [7], and other fundamental biological processes. Important aspects of oscillatory behavior include synchronization, and entrainment [8, 9, 10]. Neural disorders such as epilepsy and Parkinson's disease, for instance, are thought to result from an excess of synchronous neural activity; destabilizing these oscillations has been proposed as a treatment for pathological neuronal activity [11, 12]. A mathematical framework, particularly phase reduction, has proven to be an effective way to understand these aspects of oscillatory dynamics.

In the deterministic setting, we consider continuous-time, smooth dynamical systems. For stable limit cycles, Guckenheimer defines isochrons, level sets of the phase variable, in two equivalent manners. The first is the *asymptotic* approach considering long-term behavior: An isochron is defined as the set of the initial conditions in the basin of attraction for which trajectories will asymptotically converge to the same common trajectory on the limit cycle [13]. The second is the short-term approach considering time lapses of length equalling the period of the limit cycle: Isochrons are Poincaré sections for which the first-return time is a constant interpreted as the period [13].

It is desirable to extend this notion of phase to *stochastic* oscillators, as noise is ubiquitous in both natural and engineered systems. Two alternative definitions

of asymptotic phase for stochastic oscillators have been introduced in recent literature [1, 2]. In [2], Thomas and Lindner introduced a new spectral phase definition derived from the slowest decaying eigenfunction of the Kolmogorov backward operator. This definition is taken in the limit of arbitrarily long time, which parallels Guckenheimer’s asymptotic approach. Previously, Schwabedal and Pikovsky introduced average isophases, which are sections in state space with constant mean first-return times, as another method of phase description for stochastic oscillators [1]. Average isophases mirror Guckenheimer’s short-term approach, considering only one orbit and generalizing first-return times. In §2 I review background material on mean first-passage time problems.

A third phase description, applicable to one-dimensional stochastic oscillators, is the current model in [14]. It is a dynamical description defined by the invariant probability density. The current model obeys the deterministic equation $\dot{\theta} = H(\theta)$ where $H = J_{ss}/\rho_{ss}(\theta)$ is the stationary flux divided by the stationary density. Using this approach, the current model phase description exhibits the correct frequency and invariant distribution density of the original stochastic oscillator. I do not consider this version of “phase” further in this thesis.

Schwabedal and Pikovsky calculated average isophases using a simulation based numerical optimization scheme [1]. In that direction, we extend their definition of the “mean isophase” function by clarifying its mathematical foundations and reformulating it as the solution of a partial differential equation (PDE) with a particular boundary condition. I didactically introduce this

PDE reformulation for one-dimensional systems in §3 and for planar systems in §4.

Although the short-term and long-term notions of phase are equivalent in the deterministic setting, it is not obvious whether they should remain equivalent for stochastic systems. In §5 I will present results on the (non)equivalence of the two alternative definitions of asymptotic phase for stochastic oscillators.

1.1 Average Isophase [1]

Schwabedal and Pikovsky introduced a “phase description for stochastic oscillators” in [1]. *Average isophases*, a generalization of deterministic isophases [15], are sections in state space with constant mean first-return time. We aim here to provide a precise mathematical interpretation of Schwabedal and Pikovsky’s notion of average isophase. Therefore we begin by restating their description as it appears in [1].

We start by reminding the reader the standard definition of isophases in deterministic systems with a stable periodic orbit $\mathbf{x}_0(t) = \mathbf{x}_0(t+T)$ of period T . For these, isophases are also isochrones. First, one defines the phase on the orbit $\varphi(\mathbf{x}_0)$. When being observed stroboscopically with time interval T , all the points \mathbf{x} that converge to a particular point on the orbit \mathbf{x}_0 have the phase $\varphi(\mathbf{x}_0)$. These points form a Poincaré surface of section $J(\varphi(\mathbf{x}_0))$ for the trajectories of the dynamical system, with

the special property that the return time to this surface equals T for all points on it. Thus, finding an isophase surface is equivalent to finding a Poincaré surface of section with the constant return time T .

For a noisy system we define the isophase surface J as a Poincaré surface of section, for which the mean first return time $J \rightarrow J$, *after performing one full oscillation*, is a constant T , which can be interpreted as the average oscillation period. In order for isophases to be well defined, oscillations have to be well defined as well: for example in polar coordinates, the radius variable must never become zero, so that one can reliably recognize each “oscillation.” Random processes for which this is not the case should be treated with care.

Analytical calculations of the mean first return time (MFRT) are a complex problem in dimensions larger than one; therefore, below we apply a simple numerical algorithm for construction of the isophases: an initial Poincaré section is iteratively altered until all mean return times are approximately equal. In two-dimensional systems for which isophases are lines, we represent Poincaré sections by a linear interpolation in between a set of knots. For each knot x_j , the average return time T_j is computed via the Monte Carlo simulation. According to the mismatch of T_j and the mean period $\langle T \rangle$, the knot x_j is advanced or retarded. The procedure is repeated with all knots, until it converges and all return times T_j are nearly equal to $\langle T \rangle$. [emphasis added]

The paper [1] provides examples of average isophase computations for a wide

variety of systems. The paper does *not* address the convergence or stability of the numerical algorithm in detail. In this thesis I reformulate the average isophase construction as the solution $T(\mathbf{x})$ of a partial differential equation derived from a mean first passage time problem, thus overcoming (at least for two-dimensional systems) the analytical complexities alluded to in the third paragraph quoted above. The “average isophase” isochrons will correspond to level sets of the function $T(\mathbf{x})$, taken mod $\langle T \rangle$. Moreover, I provide an interpretation of the sample path condition “after performing one full oscillation” in the second paragraph, and attempt to put it on a firm mathematical foundation. Given our PDE and the appropriate boundary conditions, if there exists a solution then the solution’s level curves yield both the geometry and timing of the isophases. Moreover, any solution to the isophase problem obtained from Schwabedal and Pikovsky’s numerical method must satisfy our PDE.

As a point of notation, we will write \bar{T} to represent the mean period $\langle T \rangle$ under the stationary distribution of the stochastic oscillator.

2 Mean First-Passage Time Problem

The MFPT problem asks for the average time needed for a particle, governed by a stochastic process, to escape a region, through a particular boundary of that region. Given that this particle follows the general SDE given by (all

SDEs written in the Itô interpretation unless otherwise stated)

$$\frac{d\vec{x}}{dt} = A(\vec{x}) + B(\vec{x})\vec{\xi}(t) \quad (1)$$

where $\vec{\xi}(t)$ is independently, identically distributed delta-correlated white Gaussian noise with unit variance, that is, $\langle \xi_i(t)\xi_j(t') \rangle = \delta_{i,j}\delta(t-t')$. The MFPT function $T(\vec{x})$, as a function of location, satisfies the Kolmogorov backward operator \mathcal{L}^\dagger equal to an inhomogeneity term of -1 and the following boundary conditions [16]:

$$\mathcal{L}^\dagger[T] \equiv \sum_i A_i(\vec{x})\partial_i T + \frac{1}{2} \sum_{i,j} (BB^\top)_{ij}(\vec{x})\partial_i\partial_j T = -1 \quad (2)$$

$$T(\vec{x}) = 0 \quad \text{along escape/absorbing boundaries} \quad (3)$$

$$\nabla T \cdot \vec{n} = 0 \quad \text{along reflecting boundaries}$$

2.1 One-Dimensional and Planar Diffusion

For example, let's consider diffusion on the unit interval $[0, 1]$ where there are absorbing boundaries at $x = 0$ and $x = 1$. The SDE for this process is

$$\dot{x} = \sqrt{2D}\xi(t) \quad (4)$$

where each component $\xi_i(t)$ is unit-variance delta correlated Gaussian white noise satisfying $\langle \xi_i(s), \xi_j(t) \rangle = \delta_{i,j}\delta(t-s)$ and D is the diffusion constant.

The MFPT function $T(x)$ satisfies

$$D \frac{d^2}{dx^2} T = -1 \tag{5}$$

$$T(0) = T(1) = 0$$

We can solve the above MFPT differential equation by simple integration.

$$T(x) = -\frac{1}{2D} x(x-1) \tag{6}$$

In Figure 1, I plot 1D diffusion realizations and the corresponding MFPT function.

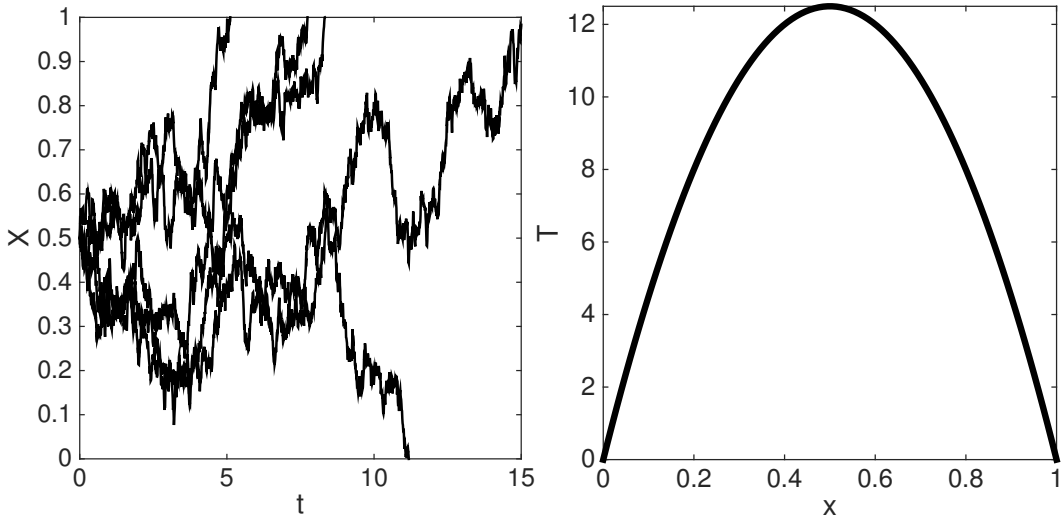


Figure 1: For one-dimensional diffusion given by (4) with $D = 0.01$ we have: (Left) 5 realizations with $X(0) = 0.5$. Note that all stochastic simulations are generated using the XPP platform [17] using the Euler-Maruyama method except as noted. (Right) MFPT function T matching (6).

For a planar example, let's consider diffusion on the unit square $\Omega = [0, 1] \times [0, 1]$ where there are absorbing boundaries on the perimeter of the square

denoted with Γ . The corresponding SDE is

$$\begin{aligned} \dot{x} &= \sqrt{2D}\xi_x(t) \\ \dot{y} &= \sqrt{2D}\xi_y(t). \end{aligned} \tag{7}$$

The MFPT function $T(x, y)$ satisfies

$$\begin{aligned} D\Delta T &= -1 \\ T(\Gamma) &= 0 \end{aligned} \tag{8}$$

We can solve the above MFPT PDE problem, given by (8), using a finite difference scheme with the following 5-point mask approximating the Laplacian operator

$$\Delta T \approx \frac{T_{i+1,j+1} + T_{i+1,j-1} - 4T_{i,j} + T_{i-1,j+1} + T_{i-1,j-1}}{h^2} \tag{9}$$

with h being the discretization size and $T_{i,j}$ referring to $T(x_i, y_j)$. In Figure 2, I plot planar diffusion realizations and the corresponding MFPT function.

3 Extending Average Isophase [1] in One-Dimension

We can use the MFPT problem framework to calculate average isophases. Identifying the correct boundary conditions is a key element of our analysis.

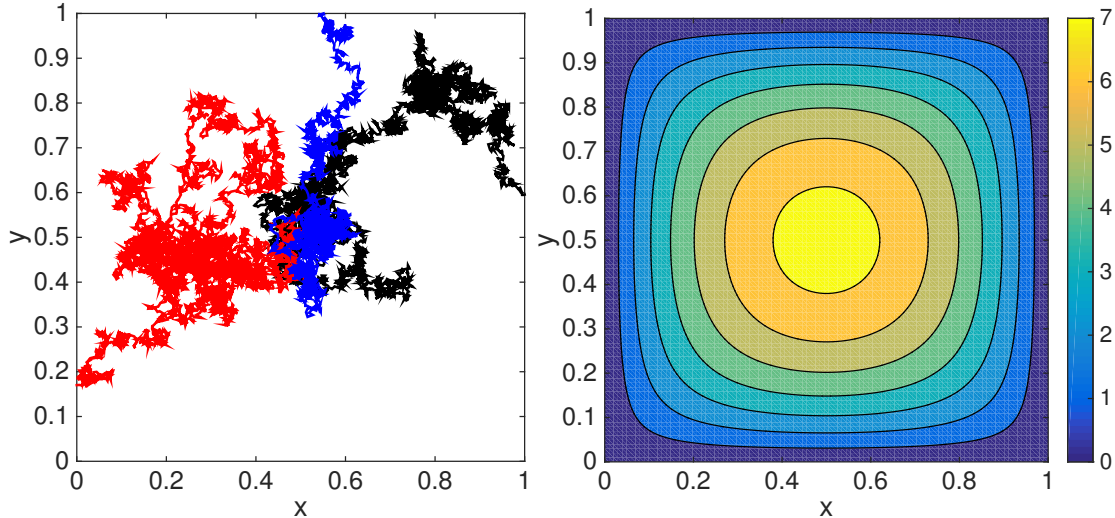


Figure 2: For planar diffusion given by (7) with $D = 0.01$ we have: (Left) 3 realizations with initial condition $(X, Y) = (0.5, 0.5)$. (Right) MFPT function T solved using finite difference scheme on a 100×100 discretization grid.

Before considering the 2D problem, first consider a 1D oscillator, realized as a stochastic process X on the circle $S \equiv [0, 2\pi)$ that obeys the SDE (10), with the coordinate x taken mod 2π .

$$\dot{x} = f(x) + \sqrt{2D(x)}\xi(t) \quad (10)$$

In this case the Fokker-Planck forward and backward operators take the form

$$\mathcal{L}[v] = -\frac{d}{dx} (f(x)v(x)) + \frac{d^2}{dx^2} (D(x)v(x)) \quad (11)$$

$$\mathcal{L}^\dagger[u] = f(x)\frac{d}{dx}u(x) + D(x)\frac{d^2}{dx^2}u(x), \quad (12)$$

where u and v are assumed to be C^2 except as noted below. We assume that $f(x)$ and $D(x)$ are periodic with period 2π .

3.1 Trivial System

First, consider the trivial stochastic oscillator of uniform drift with constant diffusion coefficient given by

$$\dot{x} = f_0 + \sqrt{2D}\xi(t), \quad (13)$$

where f_0 and D are constants. In this simple case the forward and backward operators are $\mathcal{L}[v] = -f_0v' + Dv''$, and $\mathcal{L}^\dagger[u] = f_0u' + Du''$, and the mean first passage time function must satisfy $f_0T' + DT'' = -1$. It's clear that from Schwabedal and Pikovsky's average isophase definition (described in §1.1) the MFPT function $T(x)$ from $x = 0$ to $x = 2\pi$ should be

$$T(x) = \frac{1}{f_0}(2\pi - x) \quad (14)$$

where $x = 2\pi$ is interpreted as an absorbing boundary. This means $T(0)$ is the average time needed for a trajectory with initial condition $x = 0$ to reach $x = 2\pi$ *after completing one full oscillation*. We can interpret $T(0)$ as the mean period \bar{T} . In Figure 3, I plot example trajectories of this trivial system along with its *true* MFPT function.

If we were to solve the MFPT problem on the system's natural periodic domains given by

$$T(0) = T(2\pi) = 0 \quad (15)$$

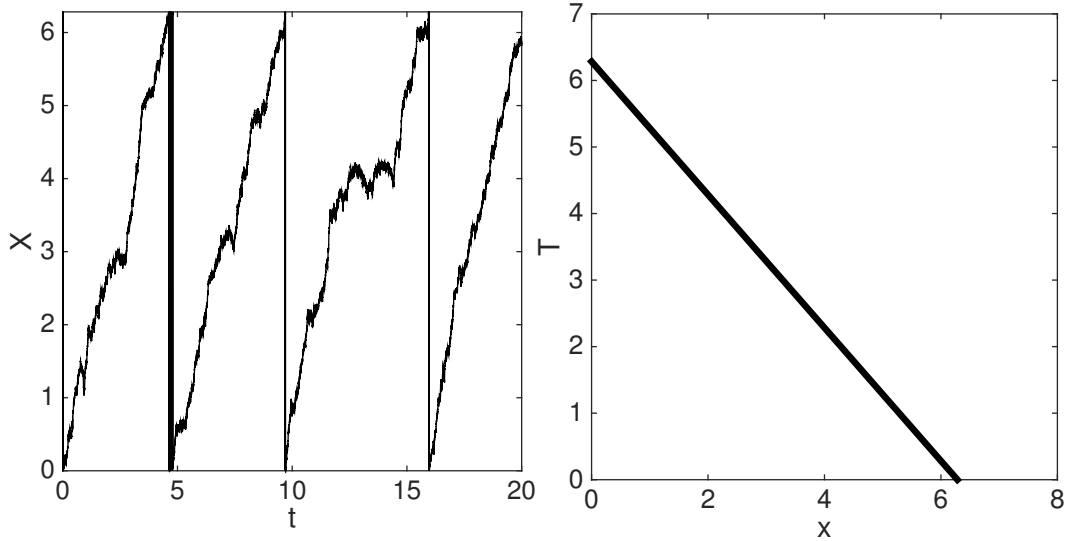


Figure 3: For the one-dimensional trivial stochastic oscillator given by (13) with $f_0 = 1$ and $D = 0.1$ we have: (Left) Realization with initial condition $X(0) = 0$. (Right) MFPT function T according to Pikovsky's average isophase definition.

we would obtain the solution plotted in Figure 4.

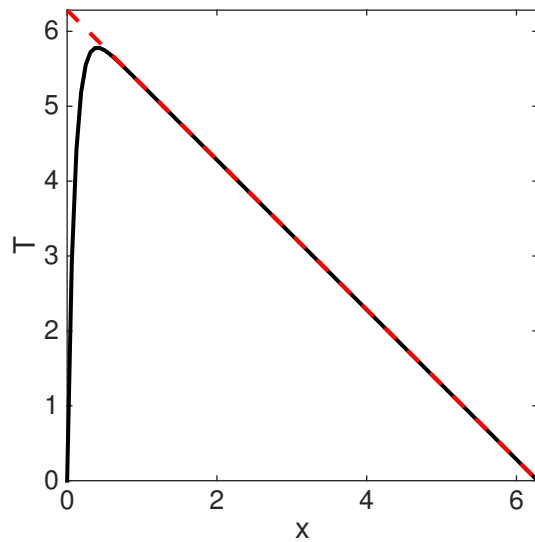


Figure 4: For the one-dimensional trivial stochastic oscillator given by (13) with $f_0 = 1$ and $D = 0.1$ we have: (Solid black line) MFPT function T solved with periodic boundary conditions using a finite difference scheme. (Dashed red line) true MFPT.

Clearly the two curves in Figure 4 don't match. The MFPT T with periodic

boundary conditions curves downward near $x = 0$ instead of remaining linear. This is because trajectories with initial conditions there can “drift backwards” into the absorbing boundary at $x = 0$. So periodic boundaries cannot be correct for calculating the average isophases. Next, we consider imposing a reflecting boundary condition at $x = 0$ while keeping an absorbing boundary at $x = 2\pi$. This forces trajectories to complete a full oscillation, in the positive direction, before being “counted”. The boundary conditions are now

$$\begin{aligned} \frac{d}{dx}T \Big|_{x=0} &= 0 \\ T(2\pi) &= 0. \end{aligned} \tag{16}$$

I plot the MFPT T for the left reflecting boundary condition in Figure 5.

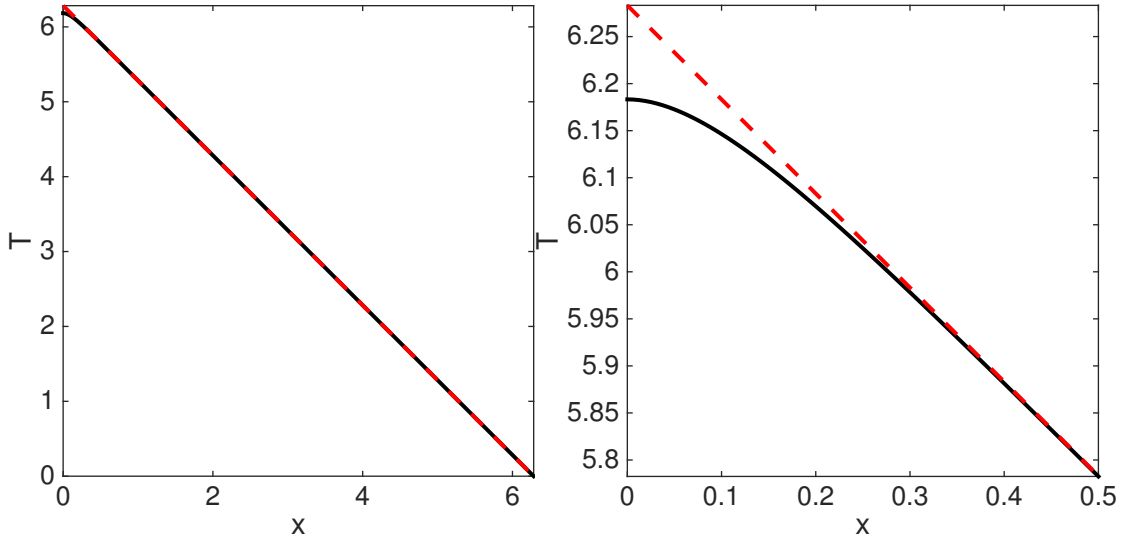


Figure 5: For the one-dimensional trivial stochastic oscillator given by (13) with $f_0 = 1$ and $D = 0.1$ we have: (Left) (Solid black line) MFPT function T solved with left reflecting boundary conditions using a finite difference scheme. (Dashed red line) ideal MFPT (Right) Zoom in of left figure near $x = 0$.

While the two functions nearly match, there is a discrepancy near $x = 0$. This

is because we have imposed a reflecting boundary there and the derivative is zero. This means trajectories that drift “backwards” through $x = 0$ because of the noise and *then* continue in the positive direction to $x = 2\pi$ will not be possible. This lowers the MFPT near $x = 0$ as seen above.

However, we could in fact extend the domain several periods backwards so that now we solve the MFPT problem on $[-2\pi n, 2\pi)$ for $n \geq 1$ where $x = -2\pi n$ is a reflecting boundary and $x = 2\pi$ remains an absorbing boundary. In this way, trajectories with initial conditions in $[0, 2\pi)$ are unlikely to be affected by the reflecting boundary at $x = -2\pi n$, given that n is sufficiently large. For practical purposes, it is enough to take $n = 2$ as the probability of a trajectory traveling backwards 2 periods to be affected by the reflecting boundary is nearly zero. To do this, we must have the assumption that $f(x)$ and $D(x)$ are *periodic* with period 2π . Below we solve the MFPT problem for the trivial system on $[-4\pi, 2\pi)$, see Figure 6.

While we still get the same discrepancy near the reflecting boundary at $x = -4\pi$, we get the correct MFPT function T on the domain of interest $[0, 2\pi)$. Now suppose we repeat this procedure on larger and larger domains, *i.e.* we take the limit as $n \rightarrow \infty$. The MFPT function $T(x)$ on each “copy” of the domain $[2\pi k, 2\pi(k+1)) \forall k$ converges, mod \bar{T} . That is, for all fixed integer $k > 0$, and for $x \in [0, 2\pi)$, $T(x)$ converges to $T(x) - k\bar{T}$ for $x \in [(-k)2\pi, (1-k)2\pi)$, in the limit as $n \rightarrow \infty$.

Thus, in a 1D scenario, following the argument above, computationally im-

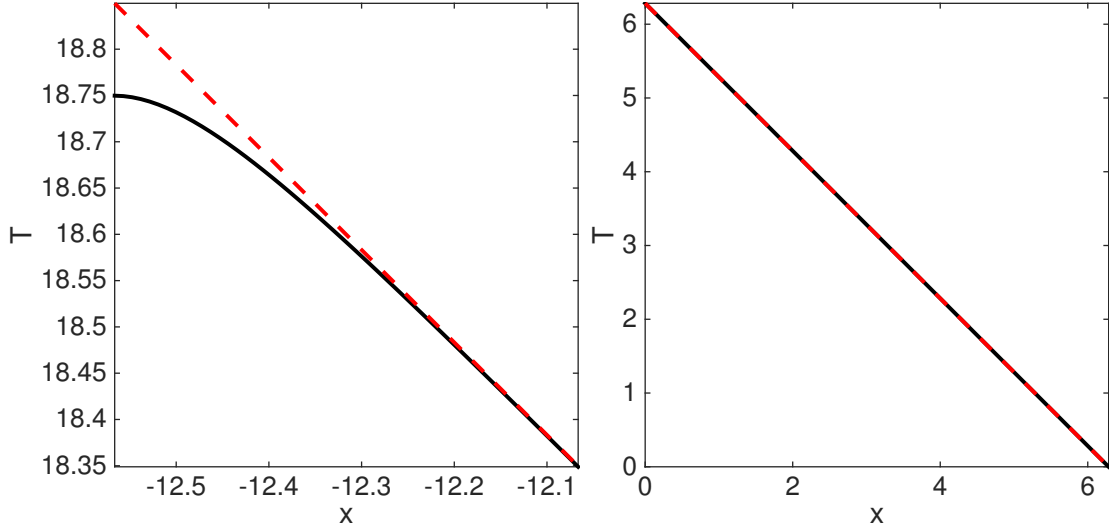


Figure 6: For one-dimensional trivial stochastic oscillator given by (13) with $f_0 = 1$ and $D = 0.1$ we have: (Left) (Solid black line) MFPT function T solved with left reflecting boundary conditions using a finite difference scheme on extended domain $[-4\pi, 2\pi)$ (Dashed red line) ideal MFPT near $x = -4\pi$. (Right) Same function on left except over actual domain of interest $[0, 2\pi)$.

posing the “full oscillation” condition from Pikovsky’s definition is a straightforward procedure. We have the boundary condition,

$$T(0) = T(2\pi) + \bar{T}. \quad (17)$$

Although from this boundary condition there is an arbitrary vertical translation, we are only interested in the level sets, which give us the average isophases. Again \bar{T} is the mean period, which can be calculated by averaging over an ensemble of Monte Carlo simulations. (See also §6.3 for an analytic approach to calculating the mean period \bar{T} , given the stationary flux.) Since there is an arbitrary vertical translation of the MFPT function $T(x)$, to avoid a singular system of equations (when solving $Ax = b$ in the finite difference

scheme) we can impose the following boundary condition instead:

$$\begin{aligned}
 T(2\pi) &= 0 && \text{absorbing at right end} \\
 T(0) &= \bar{T} && \text{full oscillation condition at left end}
 \end{aligned}
 \tag{18}$$

Figure 7 illustrates this “jump” boundary condition for the trivial 1D system.

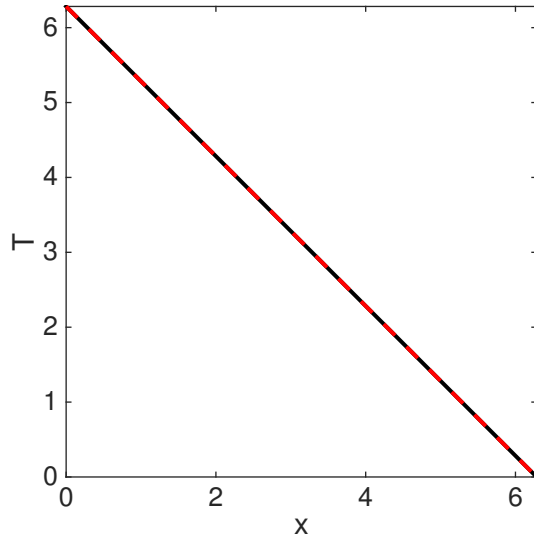


Figure 7: For one-dimensional trivial stochastic oscillator given by (13) with $f_0 = 1$ and $D = 0.1$ we have: (Solid black line) MFPT function T solved with “jump” boundary conditions using a finite difference scheme (Dashed red line) true MFPT. The point-wise error is on the order of $1e - 14$.

3.2 Tilted Periodic Potential

Next we demonstrate the equivalence of the extended domain approach and the “jump” condition for a nontrivial system: the tilted periodic potential

given by

$$\dot{x} = 1 + a \cos(x) + \sqrt{2D}\xi(t). \quad (19)$$

Without noise and for $a = 1$, the system has a fixed point at $x = \pi$. Figure 8 plots an example realization.

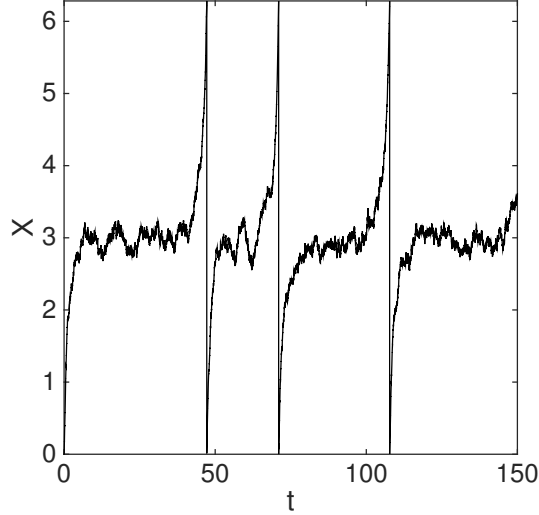


Figure 8: Realization of the tilted periodic potential given by (19) with $a = 1$ and $D = 0.01$.

For this system the forward and backward Fokker-Planck operators are $\mathcal{L}[v] = -((1 + a \cos(x))v)' + Dv''$, and $\mathcal{L}^\dagger[u] = (1 + a \cos(x))u' + Du''$. Figure 9 compares the MFPT $T(x)$ from the “jump” condition and the extended domain approach, demonstrating close agreement in this nontrivial case also.

3.3 Solvability Condition for the PDE Problem

To prove this “jump condition” with the MFPT PDE is a well-posed problem, we use the Fredholm Alternative. The linear operator version of this theorem

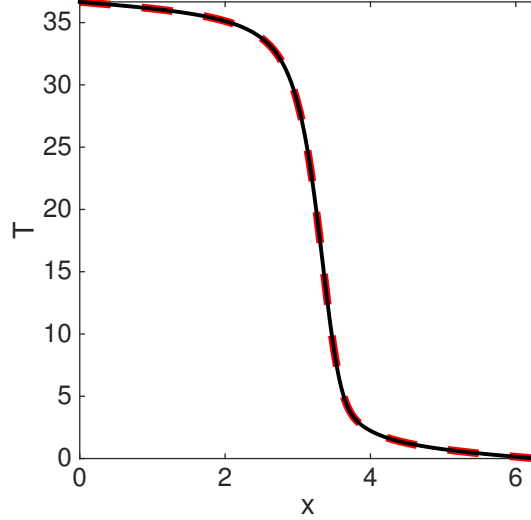


Figure 9: Tilted periodic potential given by (19) with $a = 1$ and $D = 0.01$: (Black line) MFPT with “jump” condition and (Dashed red line) MFPT with extended left reflecting boundary at $x = -4\pi$ but plotted over $[0, 2\pi)$. Point-wise error is on the order of $1e - 8$.

states (notation changed for our particular problem): Provided $b(x)$ is in the range of \mathcal{L}^\dagger , then $\mathcal{L}^\dagger[T(x)] = b(x)$ has a solution, *i.e.* the MFPT problem is well-posed, if and only if $b(x)$ is in the orthogonal complement of the nullspace of \mathcal{L} (the operator adjoint to \mathcal{L}^\dagger with respect to the standard inner product space defined by $\langle u|v \rangle = \int dx u^*(x)v(x)$). That is, for every $U(x)$ in $\ker(\mathcal{L})$, $U(x)$ and $b(x)$ are perpendicular.

Applying the Fredholm condition to our problem, we conclude that $\mathcal{L}^\dagger[T] = -1$ has a solution if and only if for every function U such that $\mathcal{L}[U] = 0$, $\langle -1, U \rangle = 0$ or $\int_0^{2\pi} dx U = 0$. This is what we will prove next. From (2), (10),

and (18) we have

$$\begin{aligned}\mathcal{L}^\dagger[T] &\equiv f(x)\frac{d}{dx}T + D(x)\frac{d^2}{dx^2}T = -1 \\ T(0) &= \bar{T} \\ T(2\pi) &= 0.\end{aligned}\tag{20}$$

The adjoint operator \mathcal{L} is defined such that $\langle \mathcal{L}^\dagger[T], U \rangle = \langle T, \mathcal{L}[U] \rangle$. The adjoint of the Kolmogorov backward operator is the forward Kolmogorov operator, also known as the Fokker-Planck operator. It is the operator appearing in the Fokker-Planck equation, which describes how the density of a stochastic process evolves in time and, for systems of the form (10), is given by

$$\mathcal{L}[U] \equiv -\frac{d}{dx}(f(x)U) + \frac{d^2}{dx^2}(D(x)U).\tag{21}$$

While we know the PDE portion of the adjoint operator, the Fokker-Planck equation above, we must calculate the corresponding boundary conditions for U from the adjoint definition itself. Once we obtain the operator \mathcal{L} , complete with the boundary conditions for U , we verify the Fredholm condition is satisfied. We apply integration by parts twice.

$$\begin{aligned}\langle \mathcal{L}^\dagger[T], U \rangle &\equiv \int_0^{2\pi} dx f(x)\frac{d}{dx}(T)U + D(x)\frac{d^2}{dx^2}(T)U \\ &= fUT \Big|_0^{2\pi} - \int_0^{2\pi} dx T \frac{d}{dx}(fU) + D(x)\frac{d}{dx}(T)U \Big|_0^{2\pi} \\ &\quad - \int_0^{2\pi} dx \frac{d}{dx}(T)\frac{d}{dx}(DU)\end{aligned}\tag{22}$$

$$\begin{aligned}
&= fUT \Big|_0^{2\pi} - \int_0^{2\pi} dx T \frac{d}{dx}(fU) + D(x) \frac{d}{dx}(TU) \Big|_0^{2\pi} \\
&\quad - T \frac{d}{dx}(DU) \Big|_0^{2\pi} + \int_0^{2\pi} dx T \frac{d^2}{dx^2}(DU) \\
&= \langle T, \mathcal{L}[U] \rangle + fUT \Big|_0^{2\pi} + D(x) \frac{d}{dx}(TU) \Big|_0^{2\pi} - T \frac{d}{dx}(DU) \Big|_0^{2\pi}
\end{aligned}$$

This means that in order for \mathcal{L} and \mathcal{L}^\dagger to be adjoint operators, the following must be true

$$fUT \Big|_0^{2\pi} + D(x) \frac{d}{dx}(TU) \Big|_0^{2\pi} - T \frac{d}{dx}(DU) \Big|_0^{2\pi} = 0. \quad (23)$$

This expression also gives us the boundary conditions for U .

Note, that $\frac{d}{dx}T$ will be periodic 2π because f, D were assumed to be 2π -periodic. Furthermore, since we assume that we are seeking a solution of the form $T(x + 2\pi) = T(x) - \bar{T}$ then dT/dx must be periodic. Plugging in the boundary conditions from (20) and taking into account the periodic functions we have

$$-f(0)\bar{T}U(0) + D(0)T'(0)[U(2\pi) - U(0)] + \bar{T}[D'(0)U(0) + U'(0)D(0)] = 0 \quad (24)$$

Because $T'(0)$ can be any arbitrary (negative) value, we must have that $U(2\pi) = U(0)$ so that the second term above is always zero. Similarly it must be the case that $U(0) = 0$ from the first term since $f(0)$ can also be any arbitrary

value and finally $U'(0) = 0$ from the last term. In other words, the only boundary condition that makes the above equation true for all systems is

$$\begin{aligned} U(0) = U(2\pi) = 0 \\ U'(0) = 0 \end{aligned} \tag{25}$$

So $\ker(\mathcal{L})$ coincides with the set of functions satisfying:

$$\begin{aligned} \mathcal{L}[U] \equiv -\frac{d}{dx}(f(x)U) + \frac{d^2}{dx^2}(D(x)U) = 0 \\ U(0) = U(2\pi) = 0 \\ U'(0) = 0 \end{aligned} \tag{26}$$

The last boundary condition $U'(0) = 0$ is redundant since the boundary conditions $U(0) = U(2\pi) = 0$ are sufficient to solve the second-order differential equation $\mathcal{L}[U] \equiv 0$. This redundancy is just a consequence of satisfying the adjoint operator definition. However, we notice that any such function U is equivalent to the steady state density of a stochastic oscillator on the circle $S \equiv [0, 2\pi)$ that obeys the SDE (10), with the coordinate x taken mod 2π . The boundary condition $U(0) = U(2\pi) = 0$ is equivalent to having an absorbing boundary there where particles are removed from the system (and can be placed in a separate “bin” to conserve probabilities). So the solution is clearly $U \equiv 0$. This satisfies the condition of the Fredholm Alternative previously stated and so this “jump condition” is indeed a well-posed problem in which at least one solution exists.

To establish uniqueness of the solution, suppose that T_1 and T_2 are distinct MFPT functions satisfying (20). Then

$$\mathcal{L}^\dagger[T_1 - T_2] = 0. \quad (27)$$

To establish uniqueness, we must prove that $\ker(\mathcal{L}^\dagger) \equiv 0$. Let $\Delta(x) = T_1(x) - T_2(x)$, and define $u(x) = d\Delta/dx$. Clearly Δ and u satisfy the boundary conditions $\Delta(0) = \Delta(2\pi) = u(0) = u(2\pi) = 0$. Moreover, Δ satisfies

$$0 = f(x)\frac{d\Delta}{dx} + D(x)\frac{d^2\Delta}{dx^2} = f(x)u(x) + D(x)\frac{du}{dx}. \quad (28)$$

Solving this differential equation yields

$$\Delta(x') = k \int_{x=0}^{x'} \exp \left[- \int_{y=0}^x \frac{f(y)}{D(y)} dy \right] dx, \quad (29)$$

for some constant $k \in \mathbb{R}$. From the boundary conditions it is clear that $k \equiv 0$, hence uniqueness is established.

4 Extending Average Isophase [1] in Planar Systems

4.1 Noisy, Heteroclinic Oscillator [2]

We didactically introduce how we extend the average isophase definition in [1] by reformulating it in terms of the MFPT PDE with a similar “jump” condition for *planar* stochastic oscillators by closely following the arguments made for one-dimensional systems. To specifically demonstrate our approach, we use a noisy, heteroclinic oscillator also used in [2, 18]. Below we specify the system,

$$\begin{aligned}\dot{x} &= f(x, y) + \sqrt{2D}\xi_1(t) \\ \dot{y} &= g(x, y) + \sqrt{2D}\xi_2(t) \\ f(x, y) &= \cos(x) \sin(y) + \alpha \sin(2x) \\ g(x, y) &= -\sin(x) \cos(y) + \alpha \sin(2y)\end{aligned}\tag{30}$$

with reflecting boundary conditions on $-\pi/2 \leq \{x, y\} \leq \pi/2$ and independent white noise sources $\langle \xi_i(t)\xi_j(t') \rangle = \delta(t-t')\delta_{i,j}$. Figure 10 displays an example trajectory, generated using the XPP platform [17].

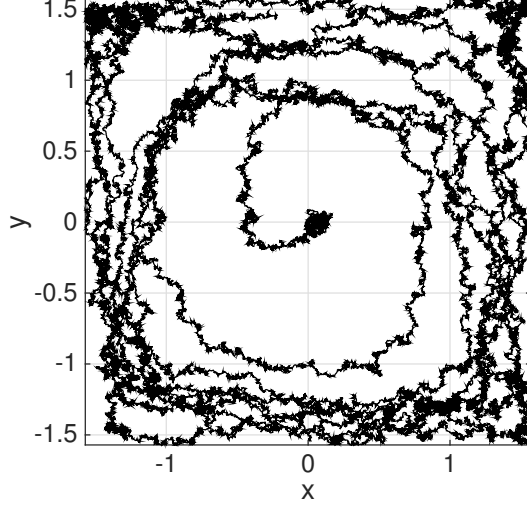


Figure 10: Trajectory with initial condition at $(0,0)$, $\alpha = 0.1$, and $D = 0.01125$. The trajectory moves clockwise. In the absence of noise, the system has a stable heteroclinic orbit with infinite period. With noise ($D > 0$), the small perturbations eventually knock the trajectory out of the corners to form a stochastic oscillator with finite mean period.

The forward and backward equations for this system are thus

$$\mathcal{L}[v] = -(\partial_x(fv) + \partial_y(gv)) + D(\partial_{xx}^2 + \partial_{yy}^2)v \quad (31)$$

$$\mathcal{L}^\dagger[u] = f\partial_x u + g\partial_y u + D(\partial_{xx}^2 + \partial_{yy}^2)u. \quad (32)$$

To reformulate the isophase calculation in terms of the MFPT PDE, we will follow a similar procedure as we did with the one-dimensional systems. In parallel with Figure (6), we can “unwrap” the oscillator so that the domain now includes multiple “periods”, which I will refer to as leaves. Similarly, the leaf, or period, of interest will contain the absorbing boundary and the “furthest backwards” leaf at the other end will contain a reflecting boundary.

Figure 11 illustrates the construction.

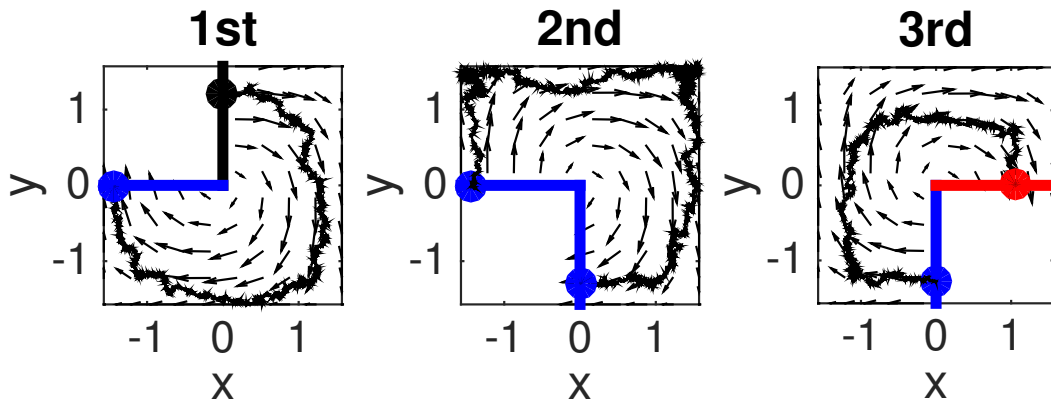


Figure 11: For the heteroclinic oscillator on an “unwrapped” domain, we consider three-quarters of the domain for each leaf for simplicity. Straight line Poincaré sections S_i are used to “connect” the leaves of this “unwrapped” oscillator. On the first leaf (left), which is the period “furthest back”, the black line S_{ref} is a reflecting boundary and we show an example trajectory originating on it. The blue line S_1 on the first leaf has a “continuity” condition with the horizontal blue line S_2 on the second leaf (middle). That is, trajectories traveling on the first leaf and through the blue section S_1 will begin on the same location on the matched blue line on the second leaf. The reverse direction is possible too and the same boundaries hold for the vertical blue line sections S_3 and S_4 on the second to third leaf (right). The red line S_{abs} on the third leaf is an absorbing boundary.

More formally, we begin with a bounded, planar, simply connected domain Ω , such as the square region in Figure 10. We assume there is a natural “center” to the domain, a point \mathbf{x}_{cent} at which the stationary flux vector field $\mathbf{J}(\mathbf{x}_{\text{cent}}) = 0$. We define the stationary flux in terms of the stationary probability density $\rho(\mathbf{x})$ as

$$\mathbf{J}(\mathbf{x}) = \mathbf{F}(\mathbf{x})\rho(\mathbf{x}) - D\nabla_{\mathbf{x}}\rho(\mathbf{x}), \quad (33)$$

where $\mathbf{F} = (f, g)^\top$ and $\mathbf{x} = (x, y)^\top$ are the velocity and position vectors, respectively. We remove a small neighborhood of \mathbf{x}_{cent} from the domain (cf. Figure 13) and take a surface of section from the outer wall to the boundary of the inner neighborhood (Figure 13, vertical blue line). We assume it is possible

to chose the section so that the stationary flux vector is transverse to it at every point along the section. Now we introduce an infinite sequence of such domains $\Omega_0, \Omega_1, \Omega_2, \dots$ and assemble a single extended domain by identifying points along one side of the cut with corresponding points along the other side of the cut lying on the next subdomain in the sequence. Thus, a point in domain Ω_k approaching the cut from the left (that is, moving in the clockwise direction) upon crossing the cut moves into domain Ω_{k-1} . This is the typical direction of motion, but because of noise, movement in the reverse direction is also possible. In this case, if a trajectory moves across the cut from right to left (that is, counterclockwise), it passes from domain Ω_k to Ω_{k+1} . The final cut at the “bottom” of domain Ω_0 is absorbing. We may compare this construction with a commercial water slide (Figure 12, right panel) as follows: most children playing on the slide move downwards, although some may (with low probability) move upwards. However, once one exits from the bottom of the last turn, there is no going back. Alternatively, one may compare the spiral surface with Winfree’s “time crystal” construction [15].

For computational purposes, we can think of this configuration on a spiral three-dimensional object with a finite number of leaves (see Figure 12).

We argue the following: that if we take the limit as the number of leaves in the three-space “time crystal” structure goes to infinity or at least very large, then the dynamics of the middle leaves are virtually non-affected by the reflecting boundary on the top leaf nor the absorbing boundary on the

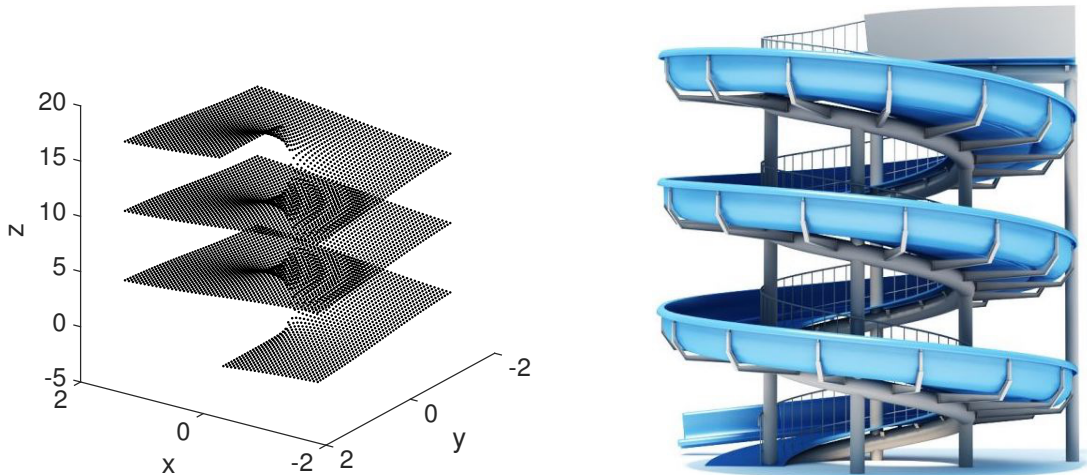


Figure 12: Left: If we were to vertically stack the multiple copies of the domain in Figure 11 and physically append the “connected” blue boundaries, we could solve the MFPT PDE on this spiraled structure. The inspiration for this structure is Winfree’s time crystal structure [15]. Right: commercial water slide (image from http://www.evermotion.org/shop/show_product/archmodels-vol-94/5828).

bottom leaf. Therefore, the middle leaves will be identical and just vertical translations of each other. In other words, they will be equivalent mod \bar{T} , as in the one-dimensional case. And thus, for the middle leaves, if we take a Poincaré section, it will be a mean period \bar{T} vertical translation from the above and below leaves.

That is we can solve the MFPT PDE for this noisy, heteroclinic oscillator using a finite difference scheme on the same square domain with reflecting boundaries with the minor modifications shown in Figure 13.

Again, we use the central difference approximation for the first-order partial derivatives and the 5-point approximation for the Laplacian operator (given by (9)). Surface and contour plots of the MFPT T are shown in Figure 14.

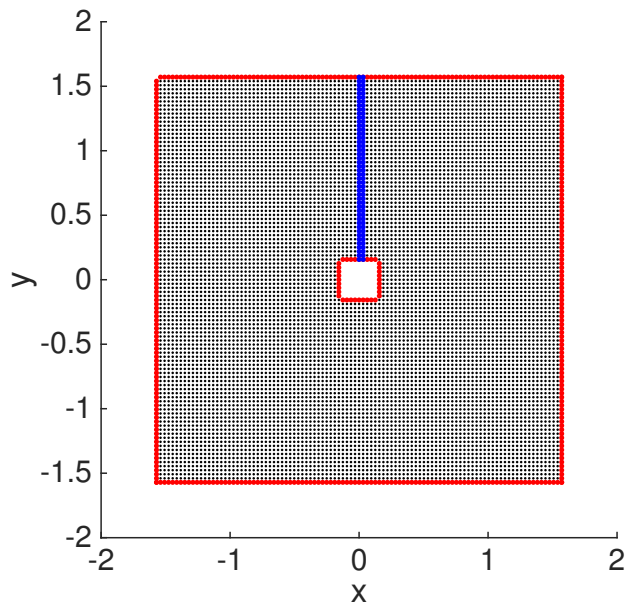


Figure 13: Black dots are nodes on the finite difference mask. Red lines represent reflecting boundaries. We implement a jump condition in parallel with (17) along the blue line, whereby subtracting \bar{T} from the nodes to right of the blue line would yield a smooth surface. We remove a small square (and impose reflecting boundaries) from the center to avoid the phase singularity there. At small noise, trajectories rarely encounter this region. Note, because there is an arbitrary vertical translation from the “jump” condition of (17), we specify the value of the northwest corner of the domain to avoid this. For the solution on the next page, we have that $T(-\pi/2, \pi/2) = 100$.

The Matlab code to calculate the MFPT and average isophases for the heteroclinic system is explicitly written in the Appendix A.1. The code reproduces Figures 13 and 14.

For this system, we do not verify that the mean first-return times of the calculated isophases is actually constant, as expected, by running Monte Carlo simulations. We only do this for the last system studied: the noisy Stuart-Landau Oscillator with y -polarized noise [1] found in §4.3.

Next I apply this method to other examples of stochastic oscillators, for ex-

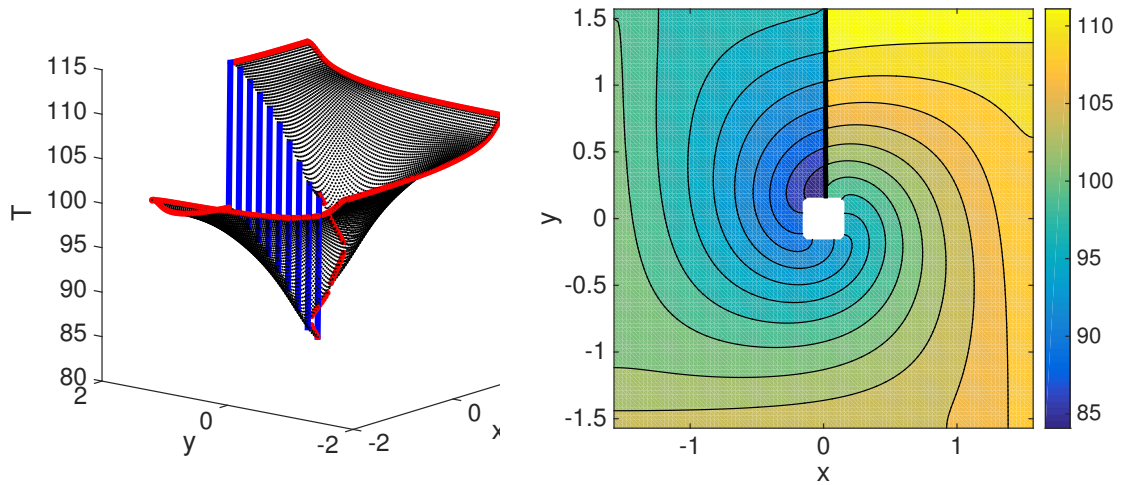


Figure 14: MFPT function T solution of finite difference scheme (described in Figure 13 for $D = 0.01125$ and side length of smaller, center square of 0.2) plotted as a (left) surface and (right) as a contour plot showing average isophases. Note that in the surface plot on the left, the colors correspond to the same boundary conditions described in Figure 13 and that the vertical blue lines are the same length corresponding to \bar{T} .

ample a generalization of the Stuart-Landau oscillator introduced in [3]. This extension of the method will require rewriting the MFPT PDE in cylindrical polar coordinates, and implementing a finite difference scheme in that coordinate system as well. The geometry then will be an annulus or punctured disk which is much more natural domain to consider oscillators on.

4.2 Generalized Stuart-Landau Oscillator [3]

From [3], a generalization of the Stuart-Landau oscillator is given by

$$\begin{aligned}\dot{x} &= -\omega y + \gamma x(1 - \rho^2) + c\gamma y Q(\rho) + \sqrt{2D}\xi_x(t) \\ \dot{y} &= \omega x + \gamma y(1 - \rho^2) - c\gamma x Q(\rho) + \sqrt{2D}\xi_y(t) \\ \rho &= \sqrt{x^2 + y^2}\end{aligned}\tag{34}$$

such that $Q(1) = 0$. The function Q determines rotation away from the deterministic limit cycle. As in their paper, we also assume that the deterministic limit cycle is strongly attracting so that $\gamma \gg \omega$ is a large parameter. Note that

$$Q_1(\rho) = \rho^2 - 1\tag{35}$$

gives the noisy Stuart-Landau system.

For the generalized Stuart-Landau oscillator, given by (34), the MFPT PDE is rewritten in cylindrical polar coordinates

$$\begin{aligned}\mathcal{L}^\dagger[T] &\equiv \left[g + \frac{D}{\rho} \right] \frac{\partial}{\partial \rho} T + f \frac{\partial}{\partial \theta} T + D \left(\frac{\partial^2}{\partial \rho^2} + \frac{1}{\rho^2} \frac{\partial^2}{\partial \theta^2} \right) T = -1 \\ f(\theta, \rho) &= \omega - \gamma c Q(\rho) \\ g(\theta, \rho) &= -\gamma \rho (\rho^2 - 1)\end{aligned}\tag{36}$$

along with the “jump” condition described in Figure 15. The terms containing D/ρ and $1/\rho^2$ are a result from the change of coordinates.

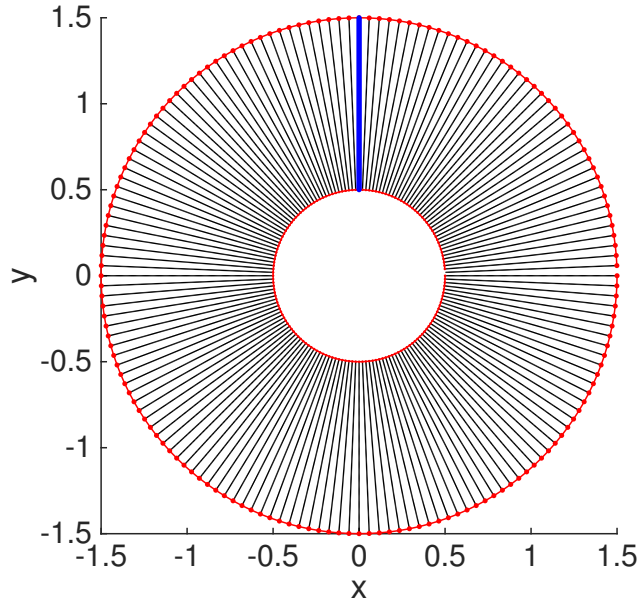


Figure 15: We solve the MFPT PDE on an annulus geometry. Black dots are nodes on the finite difference mask. Red lines represent reflecting boundaries. We implement a jump condition in parallel with (17) along the blue line, whereby adding \bar{T} from the nodes to right of the blue line would yield a smooth surface. We remove a small circle (and impose reflecting boundaries) from the center to avoid the phase singularity there. At small noise, trajectories rarely encounter this region. Similarly, trajectories rarely travel outside $r = 1.5$. Note, because there is an arbitrary vertical translation from the “jump” condition of (17), we can specify the value of the of the domain to avoid this. So for Figure 17, we have that $T(r = 0.5, \theta = 0) = 100$.

In the deterministic setting, if $c = 0$ then the system is independent of Q and reduces to a radial isochronal clock model. That is, $\dot{\theta} \equiv \text{constant } \omega$ so the isochrons will have spokes-of-a-wheel geometry. In the stochastic setting, we expect the average isophases to be the same since the noise is isotropic and of equal magnitude in both directions. Figure 16 plots an example trajectory of the isochronal clock model ($c = 0$).

Figure 17 displays the MFPT results.

From [3], two interesting oscillatory dynamics arise from (34). The first case

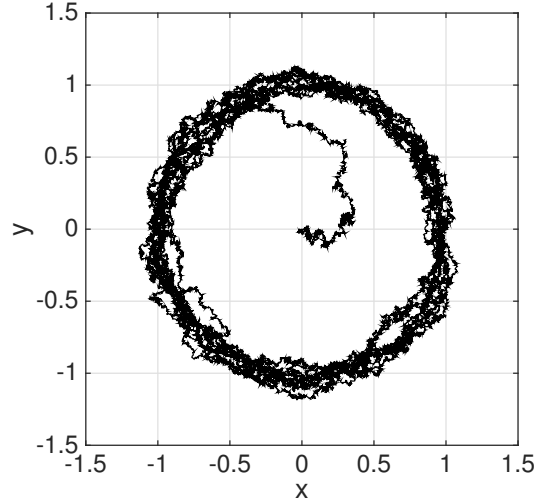


Figure 16: Trajectory of isochronal clock model with initial condition at $(0, 0)$, $\omega = 1$, $\gamma = 1$, and $D = 0.01$.

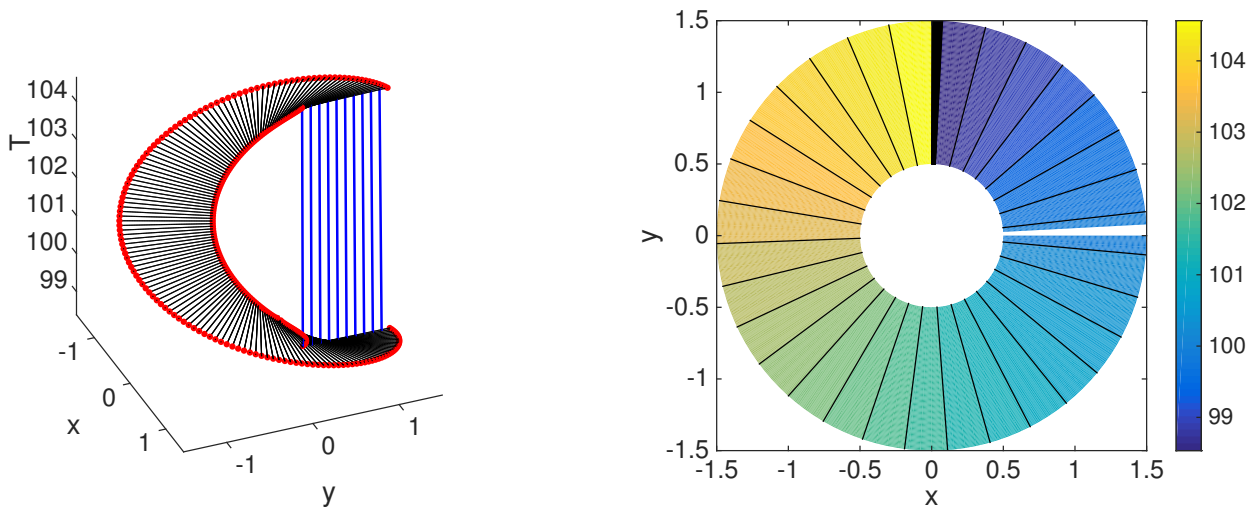


Figure 17: MFPT function T solution of finite difference scheme (described in Figure 15) for the isochronal clock model with $\omega = 1$, $\gamma = 1$, and $D = 0.01$ plotted as a (left) surface and (right) as a contour plot showing average isophases. Note that in the surface plot on the left, the colors correspond to the same boundary conditions described in Figure 15 and that the vertical blue lines are the same length corresponding to \bar{T} . As expected, the average isophases are spokes-of-the-wheel and each “spoke” is constant up to the order of $1e - 12$.

is referred to as counterrotating. Figure 18 shows an example trajectory.

The second case is referred to as antirotating and an example trajectory is

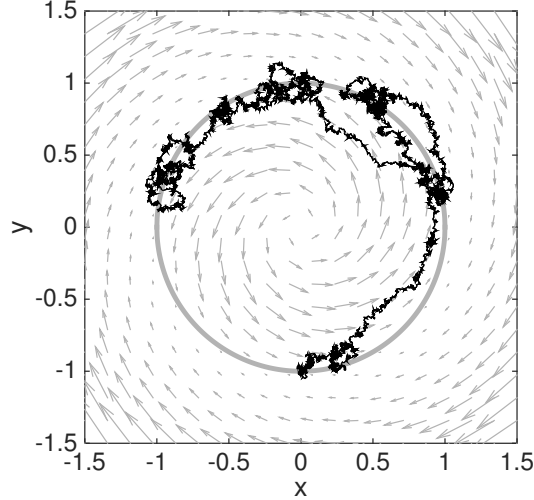


Figure 18: Trajectory of counterrotating model with initial condition at $(0, -1)$ for $Q = \rho^2 - 1$, $\omega = 1$, $\gamma = 15$, $c = 4$, and $\sqrt{2D} = 0.6$. The bolded grey circle is the deterministic limit cycle rotating counterclockwise. The grey arrows are the deterministic vector field. The vector field outside of $\rho^* = \sqrt{1 + \omega/(c\gamma)}$ rotates clockwise and rotates counterclockwise inside. Trajectories will advance around the limit cycle more quickly when inside $\rho^* = \sqrt{1 + \omega/(c\gamma)}$ and travel in the reverse direction when outside.

plotted in Figure 19.

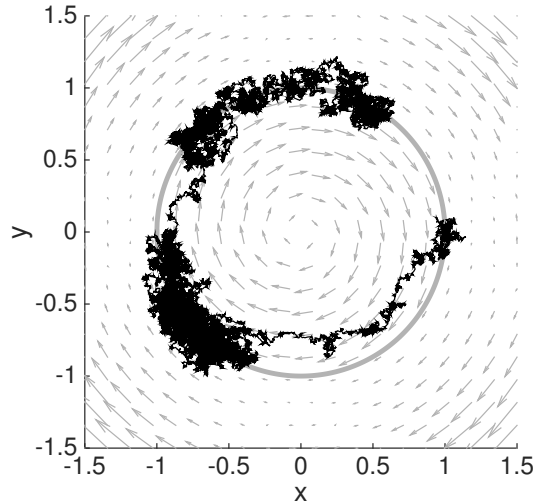


Figure 19: Trajectory of antirotating model with initial condition at $(1, 0)$ for $Q = -\omega(1 - \rho)^2$, $\omega = 1$, $\gamma = 15$, $c = -15$, and $\sqrt{2D} = 0.63$. The bolded grey circle is the deterministic limit cycle rotating counterclockwise. The grey arrows are the deterministic vector field. The vector field rotates clockwise both outside and inside of $\rho^* = 1 \pm \sqrt{1/(-c\gamma)}$ respectively. Trajectories will travel in the reverse direction as noise knocks them off the limit cycle.

We apply the same MFPT PDE finite difference approach described in Figure 15 to calculate the average isophases for these two different cases. Note that Figures 20, 21, and 24 are solved using *only* the “jump” condition at $\theta = 0$ and then the $\min(T)$ is subtracted off. When we impose the value at a single point in the finite difference scheme, the calculated MFPT T surface becomes much more sensitive to the correct value for \bar{T} . Small differences in the mean period create clearly erroneous surfaces with jagged discontinuities. For systems with larger noise, it becomes more challenging to accurately estimate the mean period \bar{T} from an ensemble of Monte Carlo simulations. With just the jump condition, the surface is less sensitive to the mean period. This makes sense as we don’t want to over-constrain the system. However, this different scheme shouldn’t affect the results.

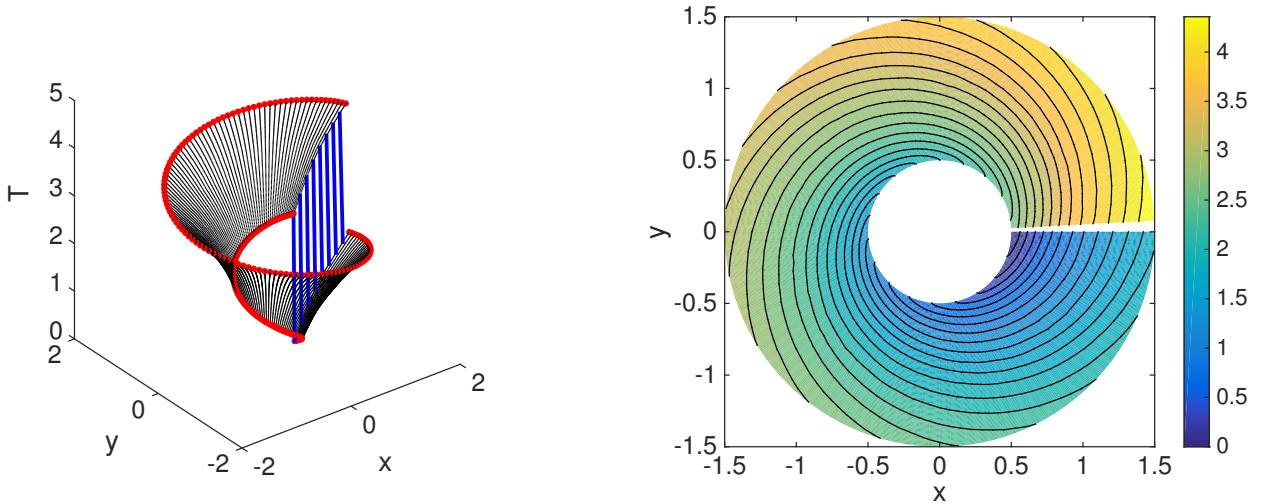


Figure 20: MFPT function T solution of finite difference scheme (described in Figure 15) for the counterrotating case with $Q = \rho^2 - 1$, $\omega = 1$, $\gamma = 15$, $c = 4$, and $\sqrt{2D} = 0.6$ plotted as a (left) surface and (right) as a contour plot showing average isophases. Note that in the surface plot on the left, the colors correspond to the same boundary conditions described in Figure 15 and that the vertical blue lines are the same length corresponding to \bar{T} .

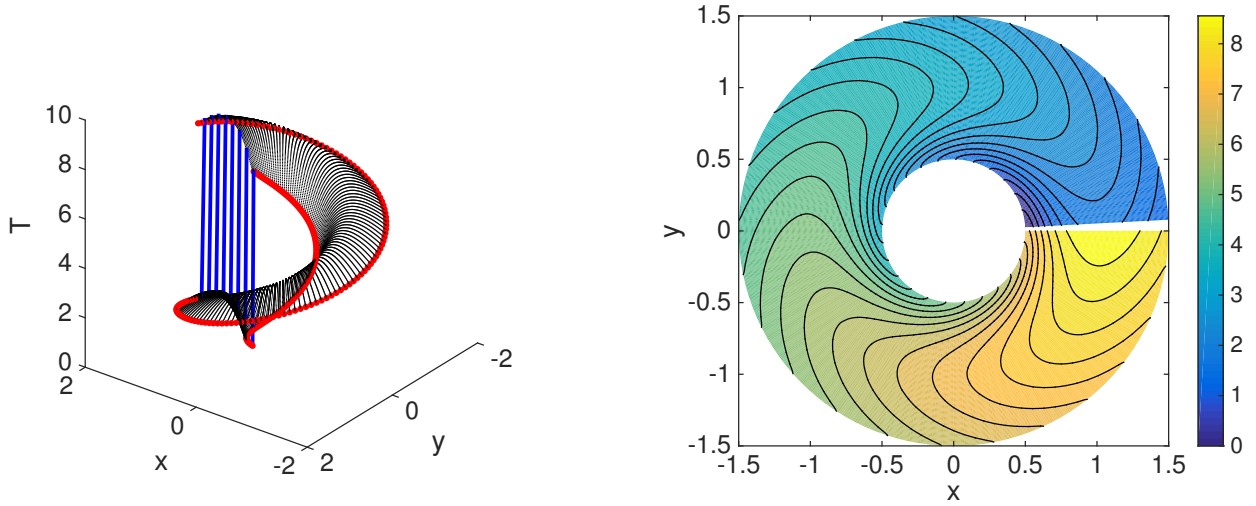


Figure 21: MFPT function T solution of finite difference scheme (described in Figure 15) for the antirotating case with $Q = -\omega(1 - \rho)^2$, $\omega = 1$, $\gamma = 15$, $c = -15$, and $\sqrt{2D} = 0.63$ plotted as a (left) surface and (right) as a contour plot showing average isophases. Note that in the surface plot on the left, the colors correspond to the same boundary conditions described in Figure 15 and that the vertical blue lines are the same length corresponding to \bar{T} .

4.3 Noisy Stuart-Landau Oscillator with y -polarized Noise

[1]

To perform noise-induced oscillations in an excitable system, [1] modifies the noisy Stuart-Landau oscillator with y -polarized noise:

$$\begin{aligned}\dot{r} &= r(1 - r^2) + \sigma r \cos \theta \circ \xi(t) \\ \dot{\theta} &= \omega + r \cos \theta - \kappa r^2 + \sigma \sin \theta \circ \xi(t).\end{aligned}\tag{37}$$

However, [1] uses the Stratonovich interpretation of SDEs, and so rewriting in the Itô interpretation, the system is then given by:

$$\begin{aligned}
 \dot{r} &= f + \sigma r \cos \theta \xi(t) \\
 \dot{\theta} &= g + \sigma \sin \theta \xi(t) \\
 f &= r(1 - r^2) + \frac{r\sigma^2}{2} (\cos^2 \theta - \sin^2 \theta) \\
 g &= \omega + r \cos \theta - \kappa r^2 + \frac{\sigma^2}{2} \cos \theta \sin \theta.
 \end{aligned} \tag{38}$$

Without noise, the system has a stable steady state so deterministic isophases do not exist. Figure 22 shows an example trajectory of this system.

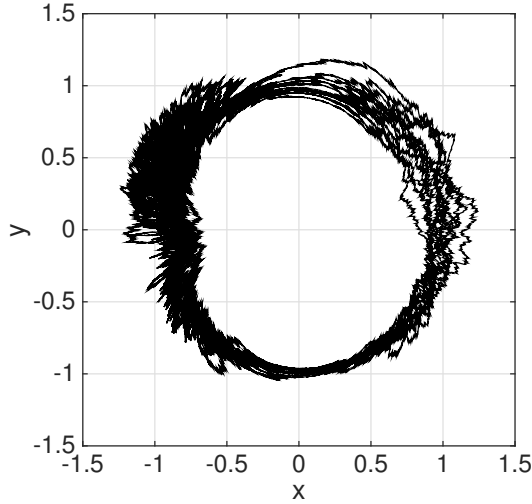


Figure 22: Example trajectory for the noisy Stuart-Landau oscillator with y -polarized noise given by (38) with $\omega = 1.99$, $\kappa = 1$, and $\sigma = 0.2$. Also note that this oscillator is *not* rotationally symmetric.

Writing the backward equation in cylindrical polar coordinates for (38) with the change of variables is cumbersome because of the multiplicative noise. Therefore, we treat the coordinates θ, r as the cartesian x, y plane, respectively.

The MFPT PDE with this coordinate system for (38) is given by

$$\begin{aligned} \mathcal{L}^\dagger[T] \equiv & f \frac{\partial}{\partial r} T + g \frac{\partial}{\partial \theta} T + \frac{1}{2} \left[\sigma^2 r^2 \cos^2 \theta \frac{\partial^2}{\partial r^2} T \right. \\ & \left. + 2\sigma^2 r \cos \theta \sin \theta \frac{\partial^2}{\partial r \partial \theta} T + \sigma^2 \sin^2 \theta \frac{\partial^2}{\partial \theta^2} T \right] = -1 \end{aligned} \quad (39)$$

$$T(r, \theta = 0) = T(r, \theta = 2\pi) + \bar{T}.$$

Figure 23, below, depicts the resulting finite difference scheme.

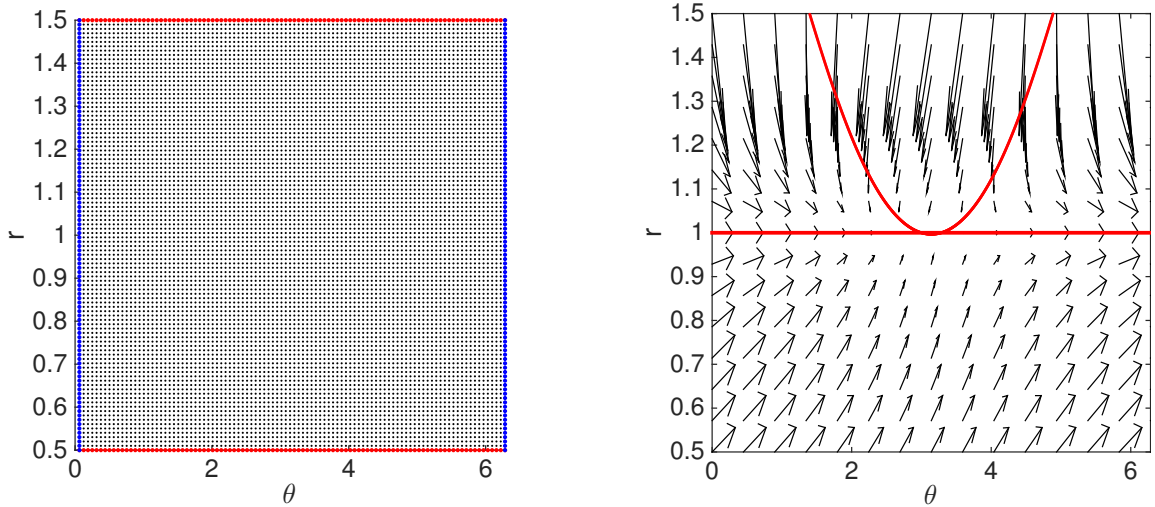


Figure 23: (Left) We solve the MFPT PDE for the noisy Stuart-Landau oscillator with y -polarized noise on the cartesian plane except with r, θ as the coordinates. Black dots are nodes on the finite difference mask. Red lines represent reflecting boundaries, corresponding with boundaries of an annulus. We implement a jump condition in parallel with (17) along the blue lines - whereby adding \bar{T} from the nodes on the left blue line would yield a smooth surface along $\theta = 0$ of the annulus. This geometry corresponds with removing a small circle (and impose reflecting boundaries) from the center to avoid the phase singularity there. At small noise, trajectories rarely encounter this region. Similarly, trajectories rarely travel outside $r = 1.5$. We solve the system with the arbitrary jump and then adjust by subtracting the $\min(T)$. (Right) Phase portrait for the *noiseless case* depicting the vector field (black arrows) and nullclines (red curves) for r (horizontal line) and θ (parabolic curve) on the same θ, r cartesian plane. For the parameters given in Fig. 22 the nullclines intersect in one stable and one unstable equilibrium point.

Figure 24 displays the MFPT solution.

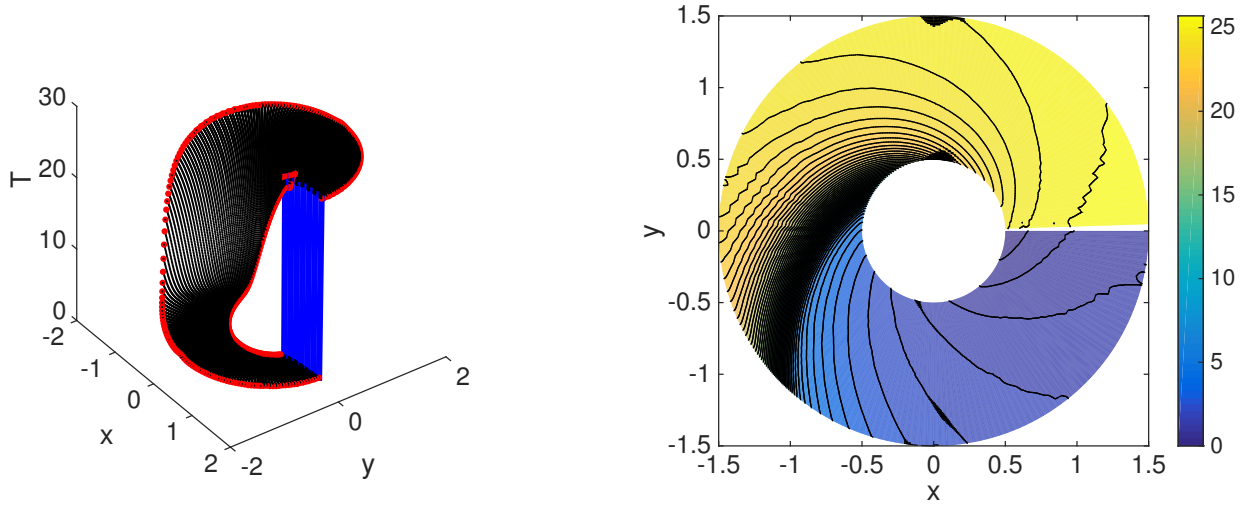


Figure 24: MFPT function T solution of finite difference scheme (described in Figure 23) for the noisy Stuart-Landau oscillator with y -polarized noise with $\omega = 1.99$, $\kappa = 1$, and $\sigma = 0.2$ plotted as a (left) surface and (right) as a contour plot showing average isophases. Note that in the surface plot on the left, the colors correspond to the same boundary conditions described in Figure 23 and that the vertical blue lines are the same length corresponding to \bar{T} .

As a further validation of my method, I ran additional Monte Carlo simulations to verify the mean first-return times (MFRT) of the calculated isophases are constant, as expected. In Figure 25, I plot an isophase and another Poincaré section of constant θ , or “wheel spoke”, overlaying an example trajectory. The “wheel spoke” is to demonstrate that the MFRT property is *not* satisfied for an arbitrary Poincaré section.

Figure 26 shows the mean first-return times for each of the initial conditions.

As you can see, simulations confirm the MFRT property of the isophase and demonstrate the MFRT property is *not* satisfied for the arbitrary “spoke” Poincaré section.

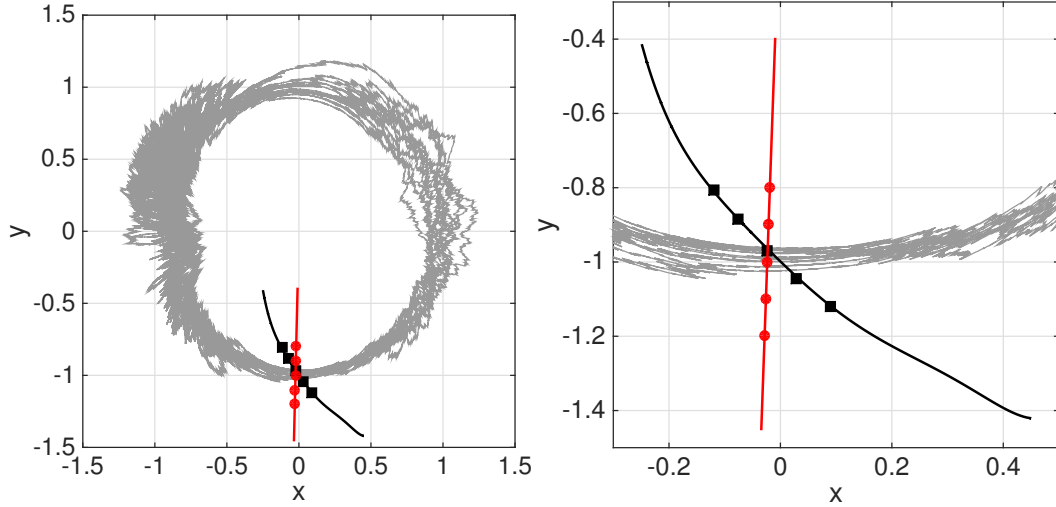


Figure 25: Example trajectory for the noisy Stuart-Landau oscillator with y -polarized noise given by (38) with $\omega = 1.99$, $\kappa = 1$, and $\sigma = 0.2$ in grey. The black curve is an isophase with five initial conditions marked by the squares. The red curve is a “spoke” through the middle isophase initial condition with five initial conditions marked by circles. The right is a zoomed-in version of the left.

4.4 Solvability Condition for the PDE Problem

Following §3.3, we prove existence of a MFPT solution T solved using our “jump” condition for planar systems with the Fredholm Alternative again.

We use the following general planar stochastic oscillator in the proof:

$$\begin{aligned}
 \dot{r} &= f(r, \theta) + \sqrt{2D_r(r, \theta)}\xi_r(t) \\
 \dot{\theta} &= g(r, \theta) + \sqrt{2D_\theta(r, \theta)}\xi_\theta(t)
 \end{aligned}
 \tag{40}$$

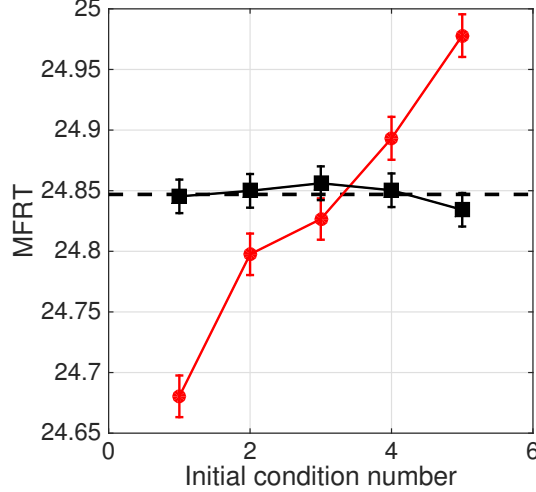


Figure 26: For each initial condition along the isophase (black curve on previous figure), Monte Carlo simulations were generated using XPP and the first-return times to the isophase, after completing a full oscillation, were calculated and averaged. A first-crossing procedure was used where the isophase was approximated using polynomial interpolation and the first time in which the trajectory crossed the polynomial in upward direction, after θ had progressed at least $3\pi/2$, was calculated. For each isophase initial condition, about 1 million trajectories are averaged for the MFRT. The first-return time for the “spoke” initial conditions was calculated by when the θ variable had advanced 2π . For each “spoke” initial condition, about 800,000 trajectories are averaged. The horizontal dashed black line is the mean period \bar{T} calculated from Monte Carlo simulations and used in the MFPT T surface calculation. The error bars are the standard error in the mean measure. We used the CWRU High Performance Cluster to perform the high volume of simulations and calculations.

on an annulus domain Ω with the boundary Γ . The boundary Γ has the following reflecting and jump conditions

$$\begin{aligned}
 \nabla T(r_{\text{outer}}) \cdot \vec{n} &= 0 \\
 \nabla T(r_{\text{inner}}) \cdot \vec{n} &= 0 \\
 T(\theta = 0) &= T(\theta = 2\pi) + \bar{T}.
 \end{aligned}
 \tag{41}$$

This setup coincides with the finite difference scheme of Figure 23. Again, we need to prove that $\iint_{\Omega} d\Omega U = 0$ where $U = \ker(\mathcal{L})$. We repeat the calculation in Section 3.3 to determine the boundary conditions for U with the \mathcal{L} operator.

First, the backward operator \mathcal{L}^\dagger and forward operator \mathcal{L} are given by

$$\begin{aligned}\mathcal{L}^\dagger[T] &\equiv f \frac{\partial}{\partial r} T + g \frac{\partial}{\partial \theta} T + D_r \frac{\partial^2}{\partial r^2} T + D_\theta \frac{\partial^2}{\partial \theta^2} T \\ \mathcal{L}[T] &\equiv -\frac{\partial}{\partial r}(fT) - \frac{\partial}{\partial \theta}(gT) + \frac{\partial^2}{\partial r^2}(D_r T) + \frac{\partial^2}{\partial \theta^2}(D_\theta T).\end{aligned}\tag{42}$$

Again, we apply integration by parts twice. For shorthand, $\vec{A} = (f, g)^\top$.

$$\begin{aligned}
\langle \mathcal{L}^\dagger[T], U \rangle &\equiv \iint_{\Omega} d\Omega U(\vec{A} \cdot \nabla T) + \iint_{\Omega} d\Omega U D_r \frac{\partial^2}{\partial r^2} T + U D_\theta \frac{\partial^2}{\partial \theta^2} T \\
&= \int_{\Gamma} d\Gamma T U(\vec{A} \cdot \vec{n}) - \iint_{\Omega} d\Omega T \nabla \cdot U \vec{A} \\
&+ \int_{\Gamma} d\Gamma \frac{\partial}{\partial r}(T) U D_r \hat{n}_r - \iint_{\Omega} d\Omega \frac{\partial}{\partial r}(T) \frac{\partial}{\partial r}(U D_r) \\
&+ \int_{\Gamma} d\Gamma \frac{\partial}{\partial \theta}(T) U D_\theta \hat{n}_\theta - \iint_{\Omega} d\Omega \frac{\partial}{\partial \theta}(T) \frac{\partial}{\partial \theta}(U D_\theta) \\
&= \int_{\Gamma} d\Gamma T U(\vec{A} \cdot \vec{n}) - \iint_{\Omega} d\Omega T \nabla \cdot U \vec{A} \\
&+ \int_{\Gamma} d\Gamma \frac{\partial}{\partial r}(T) U D_r \hat{n}_r - \int_{\Gamma} d\Gamma T \frac{\partial}{\partial r}(U D_r) \hat{n}_r \\
&+ \iint_{\Omega} d\Omega T \frac{\partial^2}{\partial r^2}(U D_r) + \int_{\Gamma} d\Gamma \frac{\partial}{\partial \theta}(T) U D_\theta \hat{n}_\theta \\
&- \int_{\Gamma} d\Gamma T \frac{\partial}{\partial \theta}(U D_\theta) \hat{n}_\theta + \iint_{\Omega} d\Omega T \frac{\partial^2}{\partial \theta^2}(U D_\theta) \\
&= \langle T, \mathcal{L}[U] \rangle + \int_{\Gamma} d\Gamma T U(\vec{A} \cdot \vec{n}) \\
&+ \int_{\Gamma} d\Gamma \frac{\partial}{\partial r}(T) U D_r \hat{n}_r - \int_{\Gamma} d\Gamma T \frac{\partial}{\partial r}(U D_r) \hat{n}_r \\
&+ \int_{\Gamma} d\Gamma \frac{\partial}{\partial \theta}(T) U D_\theta \hat{n}_\theta - \int_{\Gamma} d\Gamma T \frac{\partial}{\partial \theta}(U D_\theta) \hat{n}_\theta
\end{aligned} \tag{43}$$

This means the following terms must be equal to 0.

$$\begin{aligned}
&\int_{\Gamma} d\Gamma T U(\vec{A} \cdot \vec{n}) + \int_{\Gamma} d\Gamma \frac{\partial}{\partial r}(T) U D_r \hat{n}_r - \int_{\Gamma} d\Gamma T \frac{\partial}{\partial r}(U D_r) \hat{n}_r \\
&+ \int_{\Gamma} d\Gamma \frac{\partial}{\partial \theta}(T) U D_\theta \hat{n}_\theta - \int_{\Gamma} d\Gamma T \frac{\partial}{\partial \theta}(U D_\theta) \hat{n}_\theta = 0
\end{aligned} \tag{44}$$

Substituting in the reflecting boundary conditions from (41), the second term

cancels out and we are left with:

$$\begin{aligned} \int_{\Gamma} d\Gamma TU(\vec{A} \cdot \vec{n}) - \int_{\Gamma} d\Gamma T \frac{\partial}{\partial r}(UD_r)\hat{n}_r + \int_{\Gamma} d\Gamma \frac{\partial}{\partial \theta}(T)UD_{\theta}\hat{n}_{\theta} \\ - \int_{\Gamma} d\Gamma T \frac{\partial}{\partial \theta}(UD_{\theta})\hat{n}_{\theta} = 0 \end{aligned} \quad (45)$$

The third term, $\int_{\Gamma} d\Gamma \frac{\partial}{\partial \theta}(T)UD_{\theta}\hat{n}_{\theta}$, reduces to the left and right $\theta = 0, 2\pi$ boundaries since \hat{n}_{θ} is 0 along the horizontal $r = r_{\text{outer}}, r_{\text{inner}}$ boundaries. Because $\frac{\partial}{\partial \theta}(T)$ can be any value, it must be the case that $U(r, \theta = 0, 2\pi) = 0$. Similarly, in the first term, \vec{A} can be any arbitrary values on Γ and so $U(r = r_{\text{outer}}, r_{\text{inner}}, \theta) = 0$. This leaves the other two terms to be equal to 0, and will only be true for all solutions T if there are reflecting boundary conditions. So we finally have that \mathcal{L} and the adjoint operator are given by

$$\begin{aligned} \mathcal{L}[U] &= 0 \\ U(\Gamma) &= 0 \\ \nabla U(\Gamma) \cdot \vec{n} &= 0 \end{aligned} \quad (46)$$

As with the 1D proof, the last boundary condition $\nabla U(\Gamma) \cdot \vec{n} = 0$ is redundant since the boundary conditions $U(\Gamma) = 0$ are sufficient to solve the PDE $\mathcal{L}[U] \equiv 0$. This redundancy is just a consequence of satisfying the adjoint operator definition. Again, this is the steady state for a system where the boundaries are absorbing and so the only solution is $U \equiv 0$ and the Fredholm Alternative is satisfied. The “jump” condition is well-defined for planar systems as well.

5 (Non)Equivalence of Average Isophase [1] and Spectral Phase [2]

5.1 Spectral Phase [2]

In [2], the *spectral asymptotic phase* is derived from the spectral decomposition of the forward and backward Kolmogorov operators. Consider the conditional density $\rho(\vec{y}, t | \vec{x}, s)$ for times $t > s$, evolving according to the forward and backward equations given by:

$$\frac{\partial}{\partial t} \rho(\vec{y}, t | \vec{x}, s) = \mathcal{L}_{\vec{y}}[\rho], \quad -\frac{\partial}{\partial s} \rho(\vec{y}, t | \vec{x}, s) = \mathcal{L}_{\vec{x}}^\dagger[\rho]. \quad (47)$$

Note that $\mathcal{L}_{\vec{y}}$ and $\mathcal{L}_{\vec{x}}^\dagger$ are adjoint operators, with respect to a natural inner product. For a smooth function $f(\vec{x})$, where $\vec{x}(t)$ is given by the following stochastic differential equation (SDE), using the Itô interpretation:

$$\frac{d\vec{x}}{dt} = A(\vec{x}) + B(\vec{x})\vec{\xi}(t). \quad (48)$$

The operator $\mathcal{L}_{\vec{x}}^\dagger[f(\vec{x})]$ is:

$$\mathcal{L}_{\vec{x}}^\dagger[f(\vec{x})] = \sum_i A_i(\vec{x}) \partial_i f + \frac{1}{2} \sum_{i,j} (BB^\top)_{ij}(\vec{x}) \partial_i \partial_j f. \quad (49)$$

We assume throughout that the conditional density can be written as the following sum:

$$\rho(\vec{y}, t|\vec{x}, s) = P_0(\vec{y}) + \sum_{\lambda} \exp(\lambda(t-s)) P_{\lambda}(\vec{y}) Q_{\lambda}^*(\vec{x}) \quad (50)$$

where the eigentriples (λ, P, Q^*) satisfy:

$$\begin{aligned} \mathcal{L}[P_{\lambda}] &= \lambda P_{\lambda} \\ \mathcal{L}^{\dagger}[Q_{\lambda}^*] &= \lambda Q_{\lambda}^* \\ \langle Q_{\lambda}|P_{\lambda'} \rangle &= \int Q_{\lambda}^*(\vec{x}) P_{\lambda'}(\vec{x}) d\vec{x} = \delta_{\lambda, \lambda'}. \end{aligned} \quad (51)$$

P_0 is the stationary distribution corresponding to $\lambda = 0$. We assume that for all other eigenvalues λ , that $\text{Re}[\lambda] < 0$. This means that $\rho(\vec{y}, t|\vec{x}, s) \rightarrow P_0$ as $(t-s) \rightarrow \infty$. If for the slowest decaying eigenvalue $\lambda_1 = \mu + i\omega$, the following three conditions hold:

- (i) $\omega > 0$
 - (ii) $|\omega/\mu| \gg 1$
 - (iii) for all other eigenvalues λ' , $\text{Re}[\lambda'] \leq 2\mu$,
- (52)

then the system is referred to as *robustly oscillating*. This means that if we write the slowest decaying eigenfunctions in polar form, such that $P_{\lambda_1} = v \exp(-i\phi)$ and $Q_{\lambda_1}^* = u \exp(i\psi)$ with $u, v \geq 0$ and $\phi, \psi \in [0, 2\pi)$, then for

long times ($(t - s) \gg 1$) we obtain:

$$\frac{\rho(\vec{y}, t | \vec{x}, s) - P_0(\vec{y})}{2u(\vec{x})v(\vec{y})} \simeq \exp(\mu(t - s)) \cos[\omega(t - s) + \psi(\vec{x}) - \phi(\vec{y})] \quad (53)$$

As [2] argues, $\psi(\vec{x})$, the complex polar angle from the backward eigenfunction, provides a natural generalization of the asymptotic phase well known from the theory of deterministic oscillators. Consider two distinct densities approaching the steady state P_0 . As these two densities approach the steady state, they will show transient oscillations with period $2\pi/\omega$. The oscillations observed will be offset by the difference in their spectral phase $\psi(\vec{x})$.

In addition to developing a new procedure for calculating the average isophase surface, I address the question of equivalence (or non-equivalence) of the isophase reduction and the spectral phase reduction. In this section, I present preliminary results that suggest the two types of “phase” are *not* equivalent, except in some special cases.

5.2 (Non)Equivalence in One-Dimension

First, consider one-dimensional stochastic oscillators given in the form of (10). In this case, we have obtained a lemma stating, in effect, that the two phases coincide only in the trivial case of uniform drift with constant diffusion coefficient. To check equivalence, we insert the polar form of the eigenfunction,

$Q(x) = u(x) \exp \{-i\psi(x)\}$, and eigenvalue $\lambda = \mu - i\omega$ into the backward operator eigenvalue equation (51). Note, we impose all the same assumptions for the spectral phase definition laid out explicitly in [2].

$$\begin{aligned} \mathcal{L}^\dagger[Q] &\equiv f(x) \frac{d}{dx} Q + D(x) \frac{d^2}{dx^2} Q = \lambda Q \\ f(x) \frac{d}{dx} u \exp \{-i\psi\} + D(x) \frac{d^2}{dx^2} u \exp \{-i\psi\} &= (\mu - i\omega) u \exp \{-i\psi\} \end{aligned} \quad (54)$$

Computing the derivatives, dividing both sides by $Q = u \exp \{-i\psi\}$ (assuming $u \neq 0$) and separating real and imaginary parts gives

$$\begin{aligned} \mu &= f(x) \frac{u'}{u} + D(x) \left[\frac{u''}{u} - (\psi')^2 \right] \\ \omega &= f(x) \psi' + D(x) \left[\psi'' + 2 \frac{u' \psi'}{u} \right]. \end{aligned} \quad (55)$$

The second equation of (55) can be rewritten as

$$-1 = \mathcal{L}^\dagger \left[-\frac{1}{\omega} \psi \right] - \frac{2D(x) u' \psi'}{\omega u}. \quad (56)$$

If $D(x)u'\psi' = 0$, then $-1 = \mathcal{L}^\dagger[-\psi/\omega]$, which means that $T(x) = -\psi/\omega$ satisfies the mean first-passage time PDE, and thus the spectral phase is equivalent to the average isophase in this case. More generally, we may write the mean-first passage time $T(x)$ as

$$T = -\frac{\bar{T}}{2\pi} (\psi(x) - \psi_0), \quad (57)$$

since the mean period $\bar{T} = 2\pi/\omega$. The reference phase ψ_0 is a particular isochron that may be chosen arbitrarily. We conclude that for one-dimensional stochastic oscillators (*i.e.* given by (10)), the spectral phase and average isophase are equivalent if and only if

$$D(x)u'\psi' = 0. \tag{58}$$

If we assume that $D(x)$ is an analytic function (infinitely differentiable, and thus representable by a convergent Taylor series), then $D(x)$ must either have a countable collection of isolated zeroes, or else be identically equal to zero. Finally, we observe that ψ' cannot be equal to 0 on any open interval in $[0, 2\pi)$. If this were true then by (55), we would have $\omega \equiv 0$, contradicting the assumption of a “robustly oscillating” system [2]. This means that for (58) to hold, and thus the two phase definitions to be equivalent, u' must be equal to 0 - meaning that u is constant.

Thus we have established:

Lemma 1 *For one-dimensional stochastic oscillators (given by (10)) with additive white noise, $D(x) \equiv D$, the spectral phase and average isophase are equivalent if and only if $f(x)$ is constant.*

Proof: First we show that $f(x) = f_0$ (constant) implies equivalence. Write

the slowest decaying eigenfunction and eigenvalue as

$$Q(x) = \exp \{-ix\} \tag{59}$$

$$\lambda = -D - if_0 \tag{60}$$

Since $u \equiv 1$, the two phases are equivalent.

Next we prove that phase equivalence implies $f(x) = f_0$ (constant). Since the phases are equivalent, we know that $u' = 0$, so (55) reduce to

$$f(x) = \omega/\psi' = \omega/\sqrt{\frac{-\mu}{D}}. \tag{61}$$

Therefore, $f(x)$ equals a constant. Moreover, since we know that $\mu = -D$, this constant is $\omega = f_0$. This completes the proof.

Thus, we are able to show that in one dimension, for a broad class of stochastic oscillators, the two phase definitions never coincide except in the trivial case.

5.3 (Non)Equivalence in Planar Systems

For planar stochastic oscillators, following the same steps as §5.2, we establish a similar result. In parallel with (58), we can assert that the spectral phase

and average isophase are equivalent if and only if

$$\sum_{ij} (BB^\top)_{ij} (\partial_i \log u) (\partial_j \psi) = 0, \quad (62)$$

where BB^\top is from (49). This sum is zero if the gradient of the phase ψ and the gradient of the “potential” $\mathcal{U} = \log(u)$ are orthogonal with respect to the inner product defined by $\langle f, g \rangle = \sum_{i,j} (BB^\top)_{ij} f_i g_j$. Because $(BB^\top)_{ij}$ is symmetric with nonnegative entries, we have a well defined inner product. It is a curious observation that if a planar system has isotropic noise (that is, the noise in the x and y directions is independently and identically distributed with state-independent magnitude) then the above condition is satisfied if Q , and therefore $\log Q$, is a complex analytic function of $z = x + iy$. This condition is equivalent to requiring that the real and imaginary parts of the eigenfunction Q satisfy the Cauchy-Riemann equations.

6 Discussion

6.1 Extending Average Isophase [1]

Going back to the average isophase definition, any oscillatory system satisfying Schwabedal and Pikovsky’s criteria will also satisfy our PDE interpretation. Therefore we have an equivalent formulation with the advantage of

not requiring a technically challenging iterative numerical method. However, the most important contribution of this method is combining the problem of calculating the geometry *and* timing of the average isophases. In [1], the original method, while able to calculate the location (or geometry) of individual average isophase curves, does not provide the timing between each average isophase. Our method solves both of these problems simultaneously. This feature is especially important for *non-rotationally symmetric stochastic oscillators*, like the noisy Stuart-Landau oscillator with y -polarized noise. For these cases, finding the average isophase foliation cannot be solved by simply finding a single average isophase, greatly expediting the numerical procedure in [1].

6.2 Limitations of the PDE Approach

Although we are only concerned with white Gaussian noise in the models we study here, the average isophase definition from [1] is not limited to Markovian systems. However, our MFPT PDE method can be extended to non-Markovian systems. For systems driven by colored Gaussian noise, we could embed the method in higher dimensions. That is, we could impose the \bar{T} “jump” condition along a $(n - 1)$ dimensional sub-manifold of the system. For non-Gaussian noise, such as the channel noise in the neural oscillator model in [2], as long as the forward and backward operator are well-defined and have a biorthogonal

expansion on the space, our MFPT PDE method should apply again. One significant limitation of our PDE approach, compared to the original numerical procedure in [1], is that it's not clear how we could calculate average isophases for time-series data.

6.3 Relation Between Stationary Flux and Mean Period

There remains an open question in our MFPT approach. For the MFPT calculations in §3 and §4, we estimated the mean period for the “jump” condition by averaging over an ensemble of Monte Carlo simulations. However, we have not yet systematically investigated how small errors in the mean period \bar{T} affect the solution T .

To circumvent this issue, we propose a semi-analytic approach to calculating the mean period \bar{T} of a stochastic oscillator through the stationary density flux. Intuitively, flux is a quantity relating to particles per time and the reciprocal of which is time per particle, relating to the mean period. For one-dimensional stochastic oscillators, we can prove the relationship

$$\bar{T} J_{\text{ss}} \equiv 1 \tag{63}$$

where J_{ss} is the stationary flux. Below we define the setup and prove this relationship.

For $x \in [0, 2\pi)$, a 1D ring, suppose $\dot{x} = f(x) + \sqrt{2D(x)}\xi(t)$, with f and D being 2π -periodic C^1 and C^2 functions, respectively. The Fokker-Planck equation for the density $\rho(x, t)$ is

$$\frac{\partial \rho}{\partial t} = -\frac{\partial}{\partial x}(\rho(x, t)f(x)) + \frac{\partial^2}{\partial x^2}(\rho(x, t)D(x)) = -\frac{\partial}{\partial x}J(x, t) \quad (64)$$

where we define the probability flux $J(x, t) = \rho(x, t)f(x) - \frac{\partial}{\partial x}(\rho(x, t)D(x))$.

At steady state we have the density $\rho_{\text{ss}}(x)$ and the stationary flux

$$J_{\text{ss}} = \rho_{\text{ss}}(x)f(x) - \frac{\partial}{\partial x}(\rho_{\text{ss}}(x)D(x)) = \text{constant}. \quad (65)$$

Let T be the mean first-passage time function for arrival at $x = 2\pi$ from initial condition $x < 2\pi$. We have

$$\begin{aligned} \mathcal{L}^\dagger[T] &\equiv f(x)\frac{dT}{dx}(x) + D(x)\frac{d^2T}{dx^2}(x) = -1 \\ T(0) &= \bar{T} \\ T(2\pi) &= 0 \end{aligned} \quad (66)$$

Lemma 2 *For one-dimensional stochastic oscillators (given by (10)), the mean period \bar{T} is the reciprocal of the stationary flux J_{ss} or $\bar{T}J_{\text{ss}} \equiv 1$.*

Proof: We write E_{ss} for expectation with respect to the steady-state density

ρ_{ss} , here written ρ . Evaluate

$$\begin{aligned}
1 &= -E_{\text{ss}}[-1] \\
&= -\int_0^{2\pi} dx \left(\rho(x)f(x)\frac{dT}{dx} + \rho(x)D(x)\frac{d^2T}{dx^2} \right) \\
&= -\int_0^{2\pi} dx \rho(x)f(x)\frac{dT}{dx} + \int_0^{2\pi} dx \frac{d(\rho(x)D(x))}{dx} \frac{dT}{dx} - \left(\rho(x)D(x)\frac{dT}{dx} \right) \Big|_0^{2\pi} \\
&= -\int_0^{2\pi} dx \left(\rho(x)f(x) - \frac{d(\rho(x)D(x))}{dx} \right) \frac{dT}{dx} - \rho(0)D(0) \left(\frac{dT}{dx}(2\pi) - \frac{dT}{dx}(0) \right) \\
&= -\int_0^{2\pi} dx \left(J_{\text{ss}} \frac{dT}{dx} \right) = -J_{\text{ss}} (T(2\pi) - T(0)) = -J_{\text{ss}}(0 - \bar{T}) \\
&= \bar{T} J_{\text{ss}}
\end{aligned} \tag{67}$$

This completes the proof.

The proof relies on two observations. First, that the MFPT from $x = 0$ to $x = 2\pi$ is equivalent to the mean period \bar{T} . That is, $\bar{T} = T(0)$. Second, that derivative of the MFPT function T is 2π -periodic. These observations are explained in §3.

We are currently working to extend this result to the n -dimensional case. In that case we have

$$\frac{d\vec{x}}{dt} = A(\vec{x}) + B(\vec{x})\vec{\xi}(t) \tag{68}$$

$$\frac{\partial \rho}{\partial t} = -\nabla \cdot (\rho A) + \nabla \cdot (\nabla(BB^\top \rho)) \tag{69}$$

We should consider the steady-state flux vector

$$\vec{J} = \rho(x)A(x) - \nabla(\rho(x)BB^T(x)) \quad (70)$$

which at steady-state is a constant (in time) vector field.

We also may have to limit ourselves to *well-behaved* oscillators, leading to assumptions including a finite domain, vector field \vec{J} is circulating, \vec{J} is not everywhere zero, \vec{J} has no fixed points on boundary, and \vec{J} is orthogonal to boundary. Specifically when $n = 2$ we should be able to show that \vec{J} will have at least one zero in the interior of the domain. Suppose \vec{J} has exactly one critical point in the interior of a planar domain. If we construct a section Σ from the boundary to the critical point and compute

$$J_{\text{total}} = \int_{x \in \Sigma} dn(x) \cdot \vec{J}(x) \quad (71)$$

$$\bar{T} = 1/J_{\text{total}}$$

with $dn(x)$ the normal vector. For well-behaved oscillators, another assumption may be that $dn \cdot \vec{J}$ has one sign only. However, this condition should be satisfied for the planar systems in §4.

This quantity in (71) should be the same for every section connecting the common center point to the boundary, by conservation of probability. As in

the 1D calculation above, we have for the MFPT

$$\begin{aligned}
 -1 &= f\nabla T + \nabla^\top g\nabla T = f_1\partial_1 T + f_2\partial_2 T + g_{11}\partial_{11} T + 2g_{12}\partial_{12} T + g_{22}\partial_{22} T \\
 g &= BB^\top
 \end{aligned}
 \tag{72}$$

since $g = g^\top$. If we were to introduce the MFPT isochrons as our sections (assuming they all meet at the critical point), we may be able to setup the integral similar to the 1D case.

Unfortunately, a proof for the 2D case still remains but I numerically checked the relation between stationary flux and mean period for the planar case of the Heteroclinic oscillator. The mean period \bar{T} from Equation (71) was calculated, pictured below in Figure 27, and the result matched the mean period calculated by averaging an ensemble of Monte Carlo simulations.

6.4 (Non)Equivalence of Average Isophase [1] and Spectral Phase [2]

While we have begun to clarify the relationship between the average isophase and spectral definitions, their equivalence for planar systems still requires further investigation. Specifically, we have yet to produce a system in which we

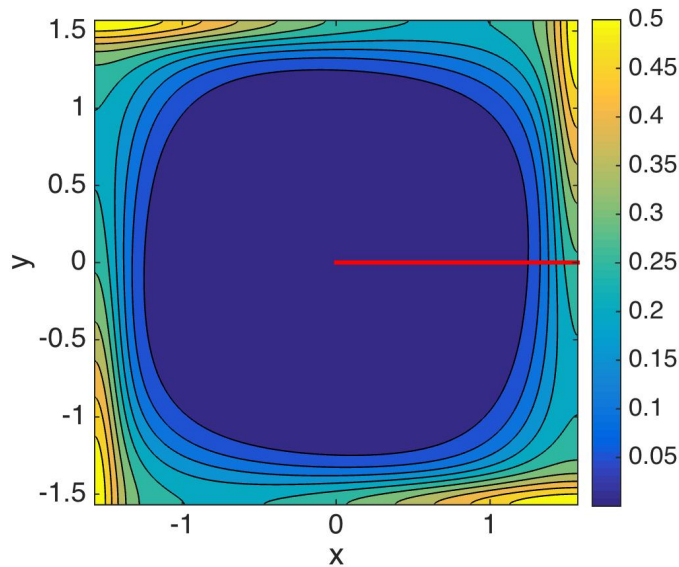


Figure 27: Stationary distribution of the Heterocline oscillator calculated in COMSOL Multiphysics. The reciprocal of the stationary flux integrated over the Poincaré section depicted with the red line, from the center of the oscillator to the boundary, matched the mean period calculated by averaging an ensemble of Monte Carlo simulations. The horizontal Poincaré section was chosen for simplicity of calculation.

could analytically calculate the backward eigenfunctions. This would allow us to confirm our derived Cauchy-Riemann condition.

7 Conclusion

In conclusion, we extended Schwabedal and Pikovsky’s average isophase definition by formulating it in terms of a partial differential equation derived from the mean first-passage time problem. Given our PDE and the appropriate boundary conditions, if there exists a solution then the solution’s level curves yield both the geometry and timing of the isophases. Moreover, any solution

to the isophase problem obtained from Schwabedal and Pikovsky's numerical method must satisfy our PDE. This formulation allows us to clarify the theoretical foundation for the average isophases, and their relation to the spectral phase.

Two alternative definitions of asymptotic phase for stochastic oscillators have been introduced in recent literature [1, 2]. We have proven that the spectral phase and average isophase generally do not coincide in one-dimensional systems. A condition for equivalence for n -dimensional systems has also been derived, relating to a n -dimensional Cauchy-Riemann sum. While these two notions of phase share similarities, the question of their equivalence remains an important open problem.

Developing a clearer understanding of the asymptotic phase for stochastic oscillators should provide a powerful tool for understanding the mechanisms of control for biological central pattern generators and other critical biological processes.

A Appendix

A.1 Matlab Code for MFPT Calculation of Heteroclinic

System [2]

```
clear

%% building geometry

% m must be odd!
m = 101; % don't change without checking figure #1
epsilon = 0.3; % don't change without checking figure #1

x = linspace(-pi/2, pi/2, m); % column stacked left to right
y = linspace(pi/2, -pi/2, m);

h = diff(x); % discretization size
h = h(1);

x_all = repmat(x, m, 1); % forming vector of ALL x coordinates in order
x_all = reshape(x_all, m^2, 1);

y_all = diag(y); % forming vector of ALL y coordinates in order
y_all = repmat(y_all, m, m);
y_all = diag(y_all);

% removing center square
remove = find(x_all > -epsilon/2 & x_all < epsilon/2 & y_all > -epsilon/2 ...
    & y_all < epsilon/2);
r = sqrt(length(remove));
x_all(remove) = [];
y_all(remove) = [];

% removing northwest corner
x_all = x_all(2:end);
y_all = y_all(2:end);

z = zeros(length(x_all), 1); % to plot geometry

% geometry plot
figure
plot3(x_all, y_all, z, 'k.', 'MarkerSize', 5)
xlabel('x')
ylabel('y')

% sorting and plotting boundaries
outer_top = find(y_all == pi/2);
hold on
```

```

plot3(x_all(outer_top), y_all(outer_top), z(outer_top), 'r.',...
      'MarkerSize', 10)

outer_bottom = find(y_all == -pi/2);
hold on
plot3(x_all(outer_bottom), y_all(outer_bottom), z(outer_bottom),...
      'r.', 'MarkerSize', 10)

outer_right = find(x_all == pi/2);
hold on
plot3(x_all(outer_right), y_all(outer_right), z(outer_right),...
      'r.', 'MarkerSize', 10)

outer_left = find(x_all == -pi/2);
hold on
plot3(x_all(outer_left), y_all(outer_left), z(outer_left), 'r.',...
      'MarkerSize', 10)

inner_top = find(x_all>=-epsilon/2 & x_all<=epsilon/2 &...
      abs(y_all-epsilon/2) <= h);
hold on
plot3(x_all(inner_top), y_all(inner_top), z(inner_top), 'r.',...
      'MarkerSize', 10)

inner_bottom = find(x_all>=-epsilon/2 & x_all<=epsilon/2 &...
      abs(y_all+epsilon/2) <= h);
hold on
plot3(x_all(inner_bottom), y_all(inner_bottom), z(inner_bottom),...
      'r.', 'MarkerSize', 10)

inner_right = find(y_all>=-epsilon/2 & y_all<=epsilon/2 &...
      abs(x_all-epsilon/2) <= h);
hold on
plot3(x_all(inner_right), y_all(inner_right), z(inner_right),...
      'r.', 'MarkerSize', 10)

inner_left = find(y_all>=-epsilon/2 & y_all<=epsilon/2 &...
      abs(x_all+epsilon/2) <= h);
hold on
plot3(x_all(inner_left), y_all(inner_left), z(inner_left),...
      'r.', 'MarkerSize', 10)

jump = find(y_all>=epsilon/2 & y_all<=pi/2 & x_all == 0);
hold on
plot3(x_all(jump), y_all(jump), z(jump), 'b.', 'MarkerSize', 10)

right_jump = find(y_all>=epsilon/2 & y_all<=pi/2 &...
      abs(x_all-h)== min(abs(x_all-h)));
hold on
plot3(x_all(right_jump), y_all(right_jump), z(right_jump),...
      'b.', 'MarkerSize', 10)
set(gca, 'FontSize', 20)
axis square

```

```

%% gathering "normal" right and left indices
right_norm = [];
for i = 1:length(y_all)-m
    if y_all(i) == y_all(i+m)
        right_norm = [right_norm i];
    end
end

left_norm = [];
for i = length(y_all):-1:(m+1)
    if y_all(i) == y_all(i-m)
        left_norm = [left_norm i];
    end
end

%% Constructing L-dagger matrix
D = 0.01125; % noise

N = length(x_all);
L_dagger = NaN(N, N);
for i = 1:N
    temp = zeros(1, N);

    temp(i) = -4 * D / h^2; % current spot

    up = i - 1; % up index
    down = i + 1; % down index

    % find if current spot is on up/down boundary
    check_outer_top = find(outer_top == i);
    check_inner_bottom = find(inner_bottom == i);
    check_outer_bottom = find(outer_bottom == i);
    check_inner_top = find(inner_top == i);

    % inserting "up" coefficient
    if length(check_outer_top) == 1
        nothing = 0;
    elseif length(check_inner_bottom) == 1
        nothing = 0;
    elseif length(check_outer_bottom) == 1
        temp(up) = 2 * D / h^2;
    elseif length(check_inner_top) == 1
        temp(up) = 2 * D / h^2;
    elseif i >= 2 % northwest corner doesn't exist
        temp(up) = g_het(x_all(i), y_all(i)) / (2*h) + D/h^2;
    end

    % inserting "down" coefficient
    if length(check_outer_bottom) == 1
        nothing = 0;
    elseif length(check_inner_top) == 1
        nothing = 0;
    elseif length(check_outer_top) == 1
        temp(down) = 2 * D / h^2;
    end
end

```

```

elseif length(check_inner_bottom) == 1
    temp(down) = 2 * D / h^2;
else
    temp(down) = -g_het(x_all(i), y_all(i)) / (2*h) + D/h^2;
end

% checking if it's in normal right/left index
check_right_norm = find(right_norm == i);
check_left_norm = find(left_norm == i);

if length(check_right_norm) == 1
    right = i + m;
else
    right = i + (m-r);
end

if length(check_left_norm) == 1
    left = i - m;
else
    left = i - (m-r);
end

% checking if on left/right boundary
check_outer_left = find(outer_left == i);
check_inner_left = find(inner_left == i);
check_outer_right = find(outer_right == i);
check_inner_right = find(inner_right == i);

% filling in coefficients
% northwest corner doesn't exist
if length(check_outer_left) == 0 &&...
    length(check_inner_right) == 0 && i >= (m+1)
    temp(left) = -f_het(x_all(i), y_all(i)) / (2*h) + D/h^2;
end

if length(check_outer_right) == 0 && length(check_inner_left) == 0
    temp(right) = f_het(x_all(i), y_all(i)) / (2*h) + D/h^2;
end

if length(check_outer_left) == 1
    temp(right) = 2*D/h^2;
elseif length(check_outer_right) == 1
    temp(left) = 2*D/h^2;
elseif length(check_inner_left) == 1
    temp(left) = 2*D/h^2;
elseif length(check_inner_right) == 1
    temp(right) = 2*D/h^2;
end

L_dagger(i, :) = temp;
disp(i/N*100)
end

%% implementing jump condition in b-vector

```

```

b = -ones(N, 1);

T_0 = 100; % specify northwest corner
b(1) = -1 - T_0 * (g_het(x_all(1), y_all(1)) / (2*h) + D/h^2);
b(m) = -1 + T_0 * (f_het(x_all(m), y_all(m)) / (2*h) - D/h^2);

T_bar = 16.225796508539315; % from simulations
b(jump) = -1 + T_bar * (f_het(x_all(jump), y_all(jump)))/(2*h) + D/h^2);
b(right_jump) = -1 + T_bar * (f_het(x_all(right_jump),...
    y_all(right_jump))/(2*h) - D/h^2);

%% solving system
T = L_dagger \ b;

%% plotting surface
figure
plot3(x_all, y_all, T, 'k.', 'MarkerSize', 5)
hold on
plot3(x_all(outer_top), y_all(outer_top), T(outer_top),...
    'r.', 'MarkerSize', 15)
plot3(x_all(outer_bottom), y_all(outer_bottom), T(outer_bottom),...
    'r.', 'MarkerSize', 15)
plot3(x_all(outer_right), y_all(outer_right), T(outer_right),...
    'r.', 'MarkerSize', 15)
plot3(x_all(outer_left), y_all(outer_left), T(outer_left),...
    'r.', 'MarkerSize', 15)
plot3(x_all(inner_top), y_all(inner_top), T(inner_top),...
    'r.', 'MarkerSize', 15)
plot3(x_all(inner_bottom), y_all(inner_bottom), T(inner_bottom),...
    'r.', 'MarkerSize', 15)
plot3(x_all(inner_right), y_all(inner_right), T(inner_right),...
    'r.', 'MarkerSize', 15)
plot3(x_all(inner_left), y_all(inner_left), T(inner_left),...
    'r.', 'MarkerSize', 15)
for i = 1:5:length(jump)
    plot3([x_all(jump(i)) x_all(right_jump(i))],...
        [y_all(jump(i)) y_all(right_jump(i))],...
        [T(jump(i)) T(right_jump(i))], 'b.-', 'LineWidth', 5)
end

xlabel('x')
ylabel('y')
zlabel('T')
set(gca, 'FontSize', 20)
axis square

%% plotting contourf
T_contour = zeros(m, m);
T_contour(remove) = NaN;

T = [T_0; T];

k = 1;
for i = 1:m^2

```

```

    if T_contour(i) == 0
        T_contour(i) = T(k);
        k = k +1;
    end
end

figure
contourf(x, x, flipud(T_contour), 15)
xlabel('x')
ylabel('y')
set(gca, 'FontSize', 20)
axis square
colorbar

:

function val = f_het(x, y)
alpha = 0.1;
val = cos(x) .* sin(y) + alpha * sin(2*x);
end

function val = g_het(x, y)
alpha = 0.1;
val = -sin(x) .* cos(y) + alpha * sin(2*y);
end

```

References

- [1] J. Schwabedal and A. Pikovsky. Phase description of stochastic oscillations. *Phys. Rev. Lett.*, 110:4102, 2013.
- [2] Peter J Thomas and Benjamin Lindner. Asymptotic phase for stochastic oscillators. *Physical review letters*, 113(25):254101, 2014.
- [3] Jay M Newby and Michael A Schwemmer. Effects of moderate noise on a limit cycle oscillator: counterrotation and bistability. *Phys Rev Lett*, 112(11):114101, Mar 2014.

- [4] Kendrick M. Shaw, David N. Lyttle, Jeffrey P. Gill, Miranda J. Cullins, Jeffrey M. McManus, Hui Lu, Peter J. Thomas, and Hillel J. Chiel. The significance of dynamical architecture for adaptive responses to mechanical loads during rhythmic behavior. *Journal of Computational Neuroscience*, in press, 2014.
- [5] Jonathan E Rubin, Bartholomew J Bacak, Yaroslav I Molkov, Natalia A Shevtsova, Jeffrey C Smith, and Ilya A Rybak. Interacting oscillations in neural control of breathing: modeling and qualitative analysis. *J Comput Neurosci*, Oct 2010.
- [6] CO Diekman, CG Wilson, and PJ Thomas. Spontaneous autoresuscitation in a model of respiratory control. *Conf Proc IEEE Eng Med Biol Soc*, pages 6669–6672, 2012.
- [7] Silvia Daun, Jonathan E Rubin, and Ilya A Rybak. Control of oscillation periods and phase durations in half-center central pattern generators: a comparative mechanistic analysis. *J Comput Neurosci*, 27(1):3–36, Aug 2009.
- [8] George Bard Ermentrout and Nancy Kopell. Frequency plateaus in a chain of weakly coupled oscillators, i. *SIAM journal on Mathematical Analysis*, 15(2):215–237, 1984.
- [9] Nathan W Schultheiss, Astrid A Prinz, and Robert J Butera. *Phase response curves in neuroscience: theory, experiment, and analysis*. Springer

- Science & Business Media, 2011.
- [10] G. Bard Ermentrout and David H. Terman. *Foundations Of Mathematical Neuroscience*. Springer, 2010.
- [11] Michele S. Titcombe, Leon Glass, Dominique Guehl, and Anne Beuter. Dynamics of Parkinsonian tremor during deep brain stimulation. *Chaos*, 11(4):766–773, Dec 2001.
- [12] Tyler Stigen, Per Danzl, Jeff Moehlis, and Theoden Netoff. Linear control of neuronal spike timing using phase response curves. *Conf Proc IEEE Eng Med Biol Soc*, 2009:1541–4, 2009.
- [13] J. Guckenheimer. Isochrons and phaseless sets. *Journal of Mathematical Biology*, 1:259–273, 1975. 10.1007/BF01273747.
- [14] Justus TC Schwabedal and Arkady Pikovsky. Effective phase description of noise-perturbed and noise-induced oscillations. *The European Physical Journal Special Topics*, 187(1):63–76, 2010.
- [15] A.T. Winfree. *The Geometry of Biological Time*. Springer-Verlag, New York, second edition, 2000.
- [16] Crispin W Gardiner et al. *Handbook of stochastic methods*, volume 3. Springer Berlin, 1985.

- [17] Bard Ermentrout. *Simulating, Analyzing, and Animating Dynamical Systems: A Guide to XPPAUT for Researchers and Students*. Society for Industrial and Applied Mathematics, 2002.
- [18] Morris W Hirsch, Stephen Smale, and Robert L Devaney. *Differential equations, dynamical systems, and an introduction to chaos*. Academic press, 2012.